

University of Southern Queensland
Faculty of Health, Engineering and Sciences

Impact Behaviour of Concrete Seawalls Reinforced with Different GFRP Bar Diameters

A dissertation submitted by

Megan Pretorius

In fulfilment of the requirements of

ENG4111/ENG4112 Research Project

Towards the degree of

Bachelor of Engineering (Honours)(Civil)

Submitted: October 2023

Abstract

In Australia, coastal regions are some of the most highly populated regions in the country. Due to the increase of extreme weather events and growing population densities along the coastline, the demand for coastal protective structures in Australia has subsequently intensified. In addressing the need for protective measures against harsh waves conditions and impact collisions from vessels, vertical concrete seawalls have been identified as an optimal design solution due to their stability and capacity to counteract horizontal impact forces.

Traditionally, steel reinforcement is used to provide the necessary tensile strength in seawalls due to the weak nature of concrete in tension. However, deterioration of reinforcement in concrete seawalls affects the structural safety and serviceability in a harmful manner. This vulnerability to corrosion from chloride in seawater makes steel a challenging design component in concrete seawalls and has prompted alternative reinforcing materials to be developed, the most prevalent being Glass Fibre Reinforced Polymer (GFRP) bars.

The primary objective of this dissertation is to provide insight into the structural performance of different GFRP bar diameters in seawalls when subjected to high impact forces during extreme weather events. This study involves experimentally testing the behaviour of concrete slabs with varying GFRP bar diameters (8mm, 10mm and 13mm) when impacted by a drop weight of 300kg. The aim is to assess the structural impact response and effectiveness of different GFRP bar diameters.

To test the slabs under simply supported conditions, an innovative test setup was designed to hold the specimens in place during the impact to reduce potential for rebound effects. The setup also allowed for the precise positioning of the 300kg drop weight directly above the slabs, ensuring consistent and centralised loading during the experiment.

To determine the optimal bar diameter, data regarding the strain, deflection, impact force and failure behaviour of the test samples were obtained and analysed. Results from this investigation were then used to conclude the impact and advantages of GFRP bar diameters with a focus on the resilience of the reinforced concrete slabs when subjected to impact loading conditions. Additionally, this research concerning the impact behaviour of GFRP reinforced concrete will further expand the applicability of this innovative material, paving the way for safer and more durable infrastructure in the future.

Limitations of Use

The Council of the University of Southern Queensland, its Faculty of Health, Engineering and Sciences, and the staff of the University of Southern Queensland, do not accept any responsibility for the truth, accuracy or completeness of material contained within or associated with this dissertation.

Persons using all or any part of this material do so at their own risk, and not at the risk of the Council of the University of Southern Queensland, its Faculty of Health, Engineering and Sciences or the staff of the University of Southern Queensland.


This dissertation reports an educational exercise and has no purpose or validity beyond this exercise. The sole purpose of the course pair entitles “Research Project” is to contribute to the overall education within the student’s chosen degree program. This document, the associated hardware, software, drawings, and any other material set out in the associated appendices should not be used for any other purpose: if they are so used, it is entirely at the risk of the user.

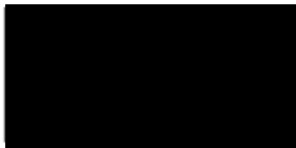
Certification of Dissertation

I certify that the ideas, designs and experimental work, results, analyses, and conclusions set out in this dissertation are entirely my own effort, except where otherwise indicated and acknowledged.

I further certify that the work is original and has not been previously submitted for assessment in any other course or institution, except where specifically stated.

Megan Pretorius

Student Number: 



Signature

15/10/23

Date

Acknowledgements

I would like to thank my supervisors, Prof Allan Manalo, Dr Omar Alajarmeh and PhD student Miss Ezgi Bal Yetim for all their support, guidance, and assistance during this research project. I am very grateful for the opportunity to be part of this research and I truly appreciate all your efforts.

I also would like to thank all UniSQ technical staff who helped me during the experimental phase of this project and UniSQ for allowing me to use their testing facilities.

Finally, I would like to thank my family and friends for all their continuous support over the past six years while I completed my studies.

Table of Contents

Abstract.....	2
Limitations of Use	3
Certification of Dissertation.....	4
Acknowledgements	5
List of Figures.....	8
List of Tables	9
Abbreviations	10
Chapter 1 Introduction.....	12
1.1 Background and Project Initiation.....	12
1.2 Project Aim.....	18
1.3 Research Significance	18
1.4 Scope.....	19
1.5 Ethics and Consequences.....	19
Chapter 2 Literature Review	20
2.1 Chapter Overview	20
2.2 Seawalls.....	20
2.2.1 General.....	20
2.2.2 A Review of Concrete Seawall Designs	21
2.3 Glass Fibre Reinforced Polymer.....	22
2.3.1 General.....	22
2.3.2 Non-Corrosive Behaviour of GFRP	23
2.3.3 Modulus of Elasticity	24
2.3.4 Flexural Performance	24
2.4 GFRP Reinforcement Standards and Specifications	26
2.5 Effect of Bar Diameter on Physical, Mechanical and Durability Properties.....	28
2.6 GFRP Bars as Reinforcement in Concrete Structures	29
2.7 Steel, GFRP & FRP Reinforced Concrete Slab Subjected to Impact Loading	31
2.8 Local and Global Response	34
2.9 Failure Mode of Steel Reinforced Concrete Slabs Subjected to Impact Loading	35
2.10 Research Gap	39
Chapter 3 Preliminary Drop Weight Testing	40
3.1 Chapter Overview	40
3.2 Specimen Details	40
3.3 Experiment Set-up	41
3.4 Test Methodology.....	43

3.5	Failure Mode Observations	43
3.5	Learnings	45
3.6	Expected Outcomes	46
Chapter 4	Official Impact Testing	47
4.1	Chapter Overview	47
4.2	Safety Considerations	47
4.3	Materials	47
4.3.1	Specimen Details	47
4.1.3	Specimen Preparation	48
4.2	Experiment Set Up	49
4.2.1	Accelerometers	51
4.2.2	Strain Gauges	52
4.2.2	Force Sensors	53
4.3	Test Methodology	53
Chapter 5	Observations, Results and Discussion	54
5.1	Chapter Overview	54
5.2	Impact Test Results	54
5.3	Impact Force	55
5.4	Energy Absorption	59
5.4	Deflection	64
5.5	Strain Data	67
5.7	Cracking Pattern and Failure Mode	71
Chapter 6	Conclusion	76
5.1	Key Project Outcomes	76
5.2	Future Work	78
	References	79
Appendices	85
	Appendix A – Project Specification	86
	Appendix B – Project Resources	87
	Appendix C – Internal Reinforcement Configurations	88
	Appendix D – Risk Assessment	90

List of Figures

Figure 1.1: Effects of Cyclone Debbie at Abel Point Marina	13
Figure 1.2: Effects of Cyclone Debbie at Shute Harbour	144
Figure 1.3: Yachts piles up at Koombana Bay Sailing Club.....	14
Figure 1.4: Ferry Crash in Canary Islands	15
Figure 1.5: Damage from Ferry Crash	15
Figure 2.1: Designs for Coastal Protection: a) Vertical Seawall, b) Curved Seawall, c) Riprap	21
Figure 2.2: Tensile Stress-Strain Curve of GFRP & Steel Bars	25
Figure 2.3: Comparison of Axial Tension Results of Steel & GFRP Reinforcement.....	25
Figure 2.4: Different Forms of Impact Damage.....	34
Figure 2.5: Flexural Mode	35
Figure 2.6: Ductile Shear	36
Figure 2.7: Shear Failure.....	36
Figure 2.8: Experimental and Analytical Load -Displacement Figure	37
Figure 2.9: Perforation and Shear Punching Transition.....	38
Figure 3.1: Test Slab Internal Reinforcement Configuration.....	40
Figure 3.2: Theoretical Test Setup.....	41
Figure 3.3: Preliminary Test Setup	42
Figure 3.4: Cracking Pattern of Preliminary Test Sample (Side Face).....	44
Figure 3.5: Cracking Pattern of Preliminary Test Sample (Bottom Face)	44
Figure 4.1: Slab Preparation at Beyond Materials Group	48
Figure 4.2: Official Testing Setup.....	50
Figure 4.3: Slab Recording Equipment Setup.....	51
Figure 4.4: Internal Strain Gauge Locations.....	52
Figure 4.5: Force Sensors and Protection Assembly	53
Figure 5.1: Force – Time Histories of S1 (Force Sensor 1)	56
Figure 5.2: Force – Time Histories of S1 (Force Sensor 2).....	56
Figure 5.3: Force – Time Histories of S2 (Force Sensor 1)	57
Figure 5.4: Force – Time Histories of S2 (Force Sensor 2)	57
Figure 5.5: Force – Time Histories of S3 (Force Sensor 1)	58
Figure 5.6: Force – Time Histories of S3 (Force Sensor 2)	58
Figure 5.7: Impact – Force Curve (S1)	60
Figure 5.8: Impact – Force Curve (S2)).....	61
Figure 5.9: Impact – Force Curve (S3)	62
Figure 5.10: 3-Phase Deformation History	64
Figure 5.11: Deflection – Time History of S1 (8mm).....	66
Figure 5.12: Deflection – Time History of S2 (10mm).....	66
Figure 5.13: Deflection – Time History of S3 (13mm)	67
Figure 5.14: Strain – Time History of S1 (8mm).....	69
Figure 5.15: Strain – Time History of S2 (10mm).....	70
Figure 5.16: Strain – Time History of S3 (13mm).....	70
Figure 5.17: Cracking Pattern of Test Slabs (Side Face).....	73
Figure 5.18: Cracking Pattern of Test Slabs (Angled View)	74
Figure 5.19: Cracking Pattern of Test Slabs (Bottom Face).....	75

List of Tables

Table 2.1: Mechanical Properties of Aslan 100 GFRP Bars.....	27
Table 2.2: Mechanical Properties of Beyond Materials Group GFRP Bars	27
Table 3.1: Set-up Components for Preliminary Testing	41
Table 4.1: Overview of Specimen Details	48
Table 4.2: Set-up Components for Official Testing.....	49
Table 5.1: Summarised Test Results.....	54
Table 5.2: 3-Phase Deflection Results	64

Abbreviations

AASHTO	American Association of State Highway and Transportation Officials
ACI	American Concrete Institute
AS 3600	Australian Standard for Concrete Structures
BFRP	Basalt Fibre Reinforced Polymer
CFM	Centre for Future Materials
CSA	Canadian Standards Association
CSA S806	Design and Construction of Building Components with Fibre Reinforced Polymers
DIC	Data Image Correlation
Dt	Change in time
F	Force
FRP	Fibre Reinforced Polymer
FTIR	Fourier Transform Infrared Spectroscopy
g	Acceleration due to gravity
GFRP	Glass Fibre Reinforced Polymer
GPa	Gigapascals
h	Drop height
J	Joules
KE	Kinetic Energy
Kg	Kilogram
kN	Kilonewton
Ku	ratio used to assess the capacity of a structural element
m	meters
mm	millimetres
MPa	Megapascals
MRTS271	TMR Technical Specification – GFRP reinforcement
N	Newtons
NSW	New South Wales
PE	Potential Energy

s	seconds
S1	Specimen 1
S2	Specimen 2
S3	Specimen 3
SEM	Scanning Electron Microscope
TMR	Transport and Main Roads
µm	Micrometres
UniSQ	University of Southern Queensland
v	Impact velocity

Chapter 1 Introduction

1.1 Background and Project Initiation

The exacerbation of extreme weather events combined with growing population densities has created the pressing necessity for effective management of coastal resources in Australia. Over 80% of the Australian population concentrated within coastal zones (Geoscience Australia 2011). Critical infrastructure such as ports, harbours and airports located in these regions, make the effects of climate change and global warming a crucial concern for Australian coastlines (Geoscience Australia 2011). According to data recorded in 2017, the Australian population amounted to 24.6 million individuals and is predicted to increase to between 37.4 and 49.2 million by 2066 (Australian Bureau of Statistics 2018). This intensifies the urgency for adequate management of coastal resources to mitigate potentially hostile repercussions.

Scientific studies have established that over the last 140 years, the average sea level has risen substantially, and projections indicate an additional increase of 1.1 meters by the year 2100 (Geoscience Australia 2011). The primary cause for the rise in sea levels can be attributed to global warming and climate change. The ocean plays a pivotal role in climate dynamics, absorbing 93% of accumulated heat in Earth's atmosphere and a quarter of the carbon dioxide (CO₂) released from the combustion of fossil fuels (NASA 2023). Data from NASA (2023) reveals that this ongoing temperature increase is leading to the melting of ice sheets which is the principal driver behind the surge in sea level. This increase in sea level leads to a range of unfavourable consequences including inundation which implies that irrespective of the ocean's behaviour, coastal zones will inevitably flood. The bathymetry and topography of the coastal margins is also projected to be severely impacted. Based on the estimate sea level rise of 1.1 meters and utilising the simple Bruun Rule for recession (recession distance equals 100 times the sea-level rise height), projections indicate that shorelines could retreat inland by approximately 55 to 100 meters. Taking into consideration Australia's current coastal population and more specifically the 6% populace residing within a 3km proximity of the shoreline, nearly 39,000 residential buildings would be lost, with approximately 40% of these structures being located in Queensland (Geoscience Australia 2011).

With the prevalent coastal population coupled with the ever-growing threat of climate change, the necessity for protecting Australian coasts has become undeniably important. In extreme weather events, the responsible selection, design, and construction of protective systems is

imperative to avoid adverse outcomes such as property damage, land loss and environmental degradation (Hosseinzadeh et al. 2022).

However, there is a major concern for steel-reinforced concrete structures in marine environments as their lifetime serviceability is notably short due to the corrosive nature of the steel reinforcement which often results to cracking and damage. This situation is intensified by the impact of rising sea-levels on coastal erosion compounded by the effect of climate change on wind strength and direction, which has implications for storm tides riding on the elevated sea levels, leading to a surge in extreme tides and waves (Hosseinzadeh et al. 2022). In such situations, seawalls are not only more susceptible to the effects of high magnitude wave action forces but are also vulnerable to the impacts of vessels crashing into the protective structures.

In 2017, the Northern Queensland region experienced the devastating effects of Cyclone Debbie. Various vessels and debris washed into Shute Harbour and Abel Point Marina in Airlie Beach, causing substantial amount of damage to the protective structures along the shoreline (ABC News 2017).



Figure 1.1: Effects of Cyclone Debbie at Abel Point Marina (ABC News 2017)

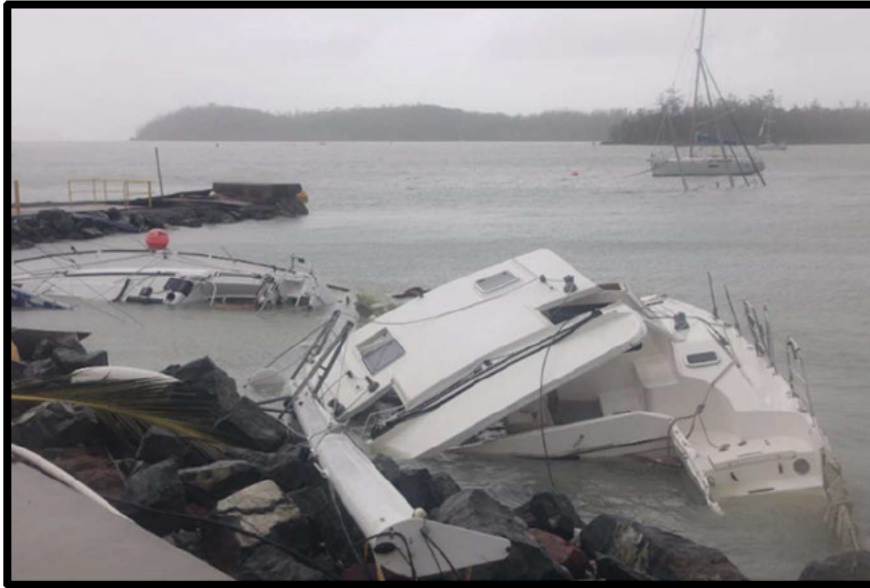


Figure 1.2: Effects of Cyclone Debbie at Shute Harbour (ABC News 2017)

The following year in 2018, the Western Australian coastline witnessed the devastating results of an extreme weather event where during a surge in tidal waves, multiple yachts broke from their mooring's. The loose yachts piled onto the shoreline at Bunbury's Koombana Bay Sailing Club (ABC News 2018).



Figure 1.3 Yachts piles up at Koombana Bay Sailing Club (ABC News 2018)

To illustrate the extent of damage a vessel can inflict on a seawall is the 2017 case of a ferry crashing into a seawall in the Canary Islands which ultimately led to a three-kilometre oil slick.



Figure 1.4: Ferry Crash in Canary Islands (The Sun 2017)

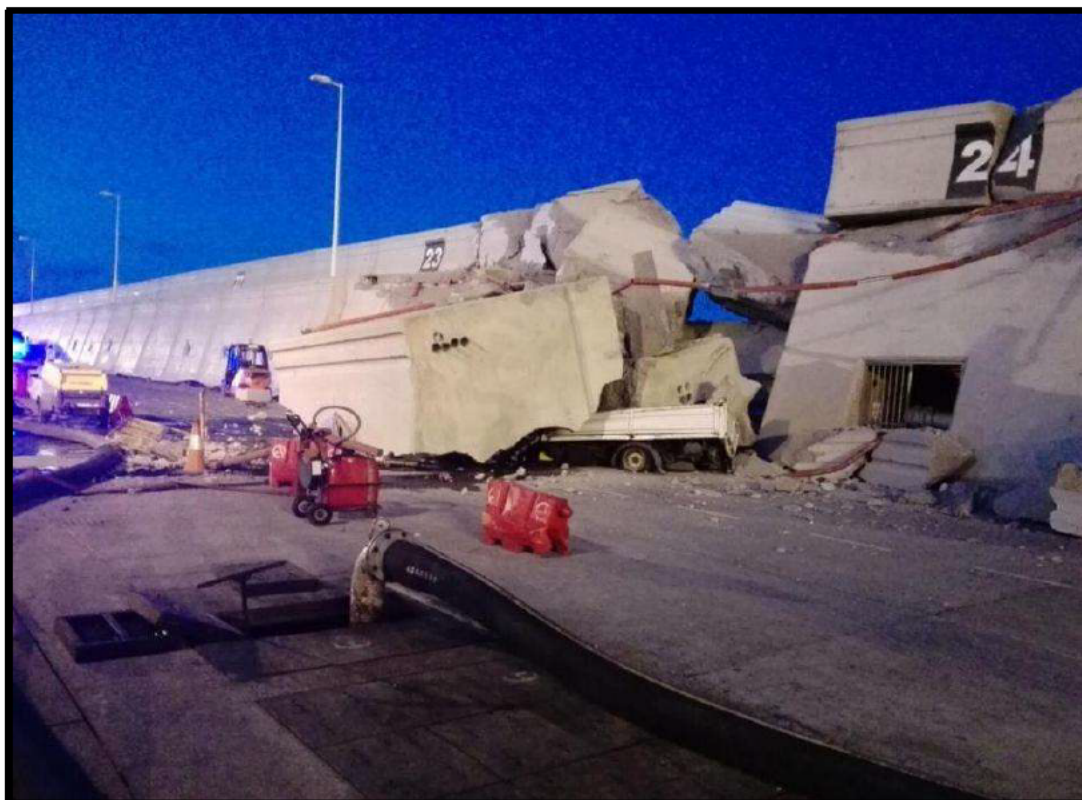


Figure 1.5: Damage from Ferry Crash (The Sun 2017)

For local governments to repair the damaged infrastructure is a costly process, resulting the infrastructure being left to age and subsequently vulnerable to further weakening and potentially ruinous failure. In 2009, St George and Sutherland Shire Council upgraded the Prince Street Seawall at Cronulla for \$4.5 million (St George and Sutherland Shire Leader 2015). Only six years later, the council requested an additional \$1 million from the federal government to repair several defects that had developed over the years. These defects included erosion, gaps between contiguous piles, exposed concrete reinforcement and subsidence of the concrete units used in the construction of the seawall (St George and Sutherland Shire Leader 2015). Research suggests that the ideal coastal structure provides protection from extreme weather events, is ecologically advanced and lasts for its intended service life without the need for excessive repair (Hosseinzadeh et al. 2022).

As for the financial implications associated with repairing corrosion-induced damage to constructed structures, the worldwide annual cost of repairs exceeds US\$1.8 trillion which translates into an average of 3% - 4% of the gross domestic product of industrialised countries (Schmitt, Schütze & Hays 2009). It is estimated that in Australia the cost to repair or replace damaged structures in 2015 was approximately AU\$13 billion per year (Cassidy, Waldie & Palanisamy 2015). The exorbitant economic burdens engendered by steel corrosion has galvanised the owners of public infrastructure to seek extended service life, increased environmental resilience and augmented economic sustainability for structures situated in coastal regions (Yang et al 2023). This collective pursuit is emblematic of an overarching commitment to mitigate financial losses and ensure the long-term viability of important marine infrastructure (Yang et al 2023).

Due to the weak nature of concrete in tension, steel reinforcement is used to provide the needed tensile strength. However, deterioration of reinforcement in concrete seawalls affects the structural safety and serviceability in a harmful manner. When steel is embedded in concrete and the covering concrete cracks, chloride ingress begins. This vulnerability to corrosion from chloride in the seawater makes steel a challenging design component in concrete seawalls that have a long service life with minimal maintenance in harsh marine environments (Chapman & Underwood 2011, pp.302-313).

The susceptibility and vulnerability of steel to chloride corrosion has prompted extensive investigations into alternative reinforcing materials. As a result, various fibre reinforced polymer (FRP) materials have been developed by researchers, the most prevalent being Glass

Fibre Reinforced Polymer (GFRP) reinforcement bars. With their noncorrosive nature, high tensile strength, light weight, and non-magnetic properties, GFRP bars emerge as a promising and effective substitute for conventional steel reinforcement in marine concrete structures (Manalo et al. 2022).

To assess the feasibility of GFRP bars as concrete reinforcement, academics have completed various comprehensive studies. A considerable proportion of this research has concentrated on examining the flexural behaviour of GFRP reinforced concrete. Flexural tests assess a material's ability to resist bending and has consistently demonstrated the capacity of GFRP bars to provide adequate tensile strength while mitigating issues associated with chloride corrosion (Shrivastava 2018). Similarly, investigations into the shear behaviour of GFRP reinforced concrete have revealed the materials capability to withstand lateral forces and maintain structural integrity. This research has highlighted GFRP's ability to distribute shear loads effectively, reducing the likelihood of shear failure and increasing the overall performance of concrete structures in shear-critical applications. Furthermore, in the realm of torsional behaviour, GFRP bars have exhibited remarkable promise as a reliable reinforcement option. Torsion, often encountered in various structural configurations such as bridges and beams, has been studied extensively and demonstrates GFRP's capacity to resist torsional forces and contribute to the overall strength and stability of the structure.

Although there is a wealth of research relating to the flexural, shear and torsional behaviour of GFRP bars, it is important to note that there remains a noticeable gap in the understanding of GFRP-reinforced concrete's response to impact loading. Impact resistance is a crucial aspect of structural performance, particularly in regard to this research that focuses on the behaviour of seawalls when subjected to impact forces during extreme weather events (Siewert et al. 2002).

The number of studies dedicated to investigating the impact behaviour of GFRP-reinforced concrete is limited. This deficiency in research stresses the need for further exploration and evaluation of GFRP-reinforced concrete under dynamic and impact loading conditions to comprehensively assess its suitability for diverse structural applications. Addressing this knowledge gap concerning the impact behaviour of GFRP reinforced concrete will further expand the applicability of this innovative material, paving the way for safer and more durable infrastructure in the future.

1.2 Project Aim

The aim of this research project is to evaluate the structural performance of different GFRP bar diameters within concrete slabs when they are subjected to an impact load. To determine the optimal bar diameter, an experimental investigation will be completed and used to obtain data regarding the strain, deflection, impact force and failure behaviour of the test samples. Results from this investigation will be used to conclude the impact and advantages of GFRP bar diameters with a focus on the resilience of the concrete slabs subjected to impact loads. An overview of the research objectives of this investigation are as follows;

- a) Review existing literature pertaining to the behaviour of reinforcement subjected to impact loads and the use of GFRP bars in concrete structures used for marine environments.
- b) Experimental testing to investigate the effect of the varying bar diameters under impact loading conditions by increasing the bar diameters used within the test specimens.
- c) Analyse the tested behaviour and mechanism of failure of the concrete slabs.

1.3 Research Significance

Seawalls are effective protective structures that are critical to the survival of Australian coastlines. Findings from this investigation have the potential to benefit up to 80% of the population currently residing within the coastal zones. If successful, GFRP reinforced concrete seawalls will aid local governments in managing the long-term maintenance issues currently undermining the performance of seawalls.

As there is currently no standard in Australia to govern the use of fibre composite reinforcement in concrete structures, further testing relating to GFRP reinforcement is required in Australia to fully grasp the depth of this alternative options capability. This research project poses as an advantageous opportunity to further explore GFRP and its performance compared to traditional steel reinforcement.

It is expected that although this investigation will be completed in accordance with Australian standards, any technical advancement made throughout the experiment can easily be adapted to satisfy the requirements of international standards.

1.4 Scope

The scope of this research project will be confined to an undergraduate level of data analysis, focusing primarily on examining the structural behaviour of varying GFRP bar diameters of 8mm, 10mm and 13mm when subjected to a drop weight of 300kg.

1.5 Ethics and Consequences

To ensure all findings within this research project are consistent and true, the report will be covered by a number of ethical publication standards. This is an undergraduate research project and therefore official publication of this report is restricted by the University of Southern Queensland. Accurate referencing will be used throughout the report to ensure that all findings are credible and reliable. This ensures a high level of authenticity and legally satisfies the requirements of giving others credit for their work and ideas. Harvard AGPS is the chosen referencing style for this report.

Chapter 2

Literature Review

2.1 Chapter Overview

This chapter will critically analyse many sources of literature related to seawall designs, GFRP and steel material properties and research concerning impact testing. This chapter will also be used to identify a research gap and explain the feasibility of this particular research project.

2.2 Seawalls

2.2.1 General

Coastal protection structures are generally constructed on the shoreline and consist of a variety of structures such as seawalls, breakwaters, jetties etc. These coastal structures can be differentiated as either “hard” or “soft structures”; with hard structures being generally not erodible, while soft structures are usually eroded by the ocean (Hosseinzadeh et al. 2022). The aim of these structures includes reducing wave impacts, flooding, and coastline erosion. Additionally, other purposes involve protecting boat traffic and stabilising navigation channels (Hosseinzadeh et al. 2022).

As for trusted solutions for coastal protection structures, seawalls are commonly employed. Generally, seawalls are long steel reinforced concrete structures, and their primary purpose is to absorb wave action, prevent coastal erosion and mitigate minor and severe flooding events. Due to wave breaking and overtopping during storm surges, seawalls are subjected to wave actions of high magnitude forces (Hosseinzadeh et al. 2022). Additionally, significant amounts of sediments are shifted as the waves reflect off the wall, causing an undesirable amount of scouring at the toe of the seawall (Pullet et al. 2007). Figure 2.1 depicts three common seawall designs typically constructed to protect shorelines.

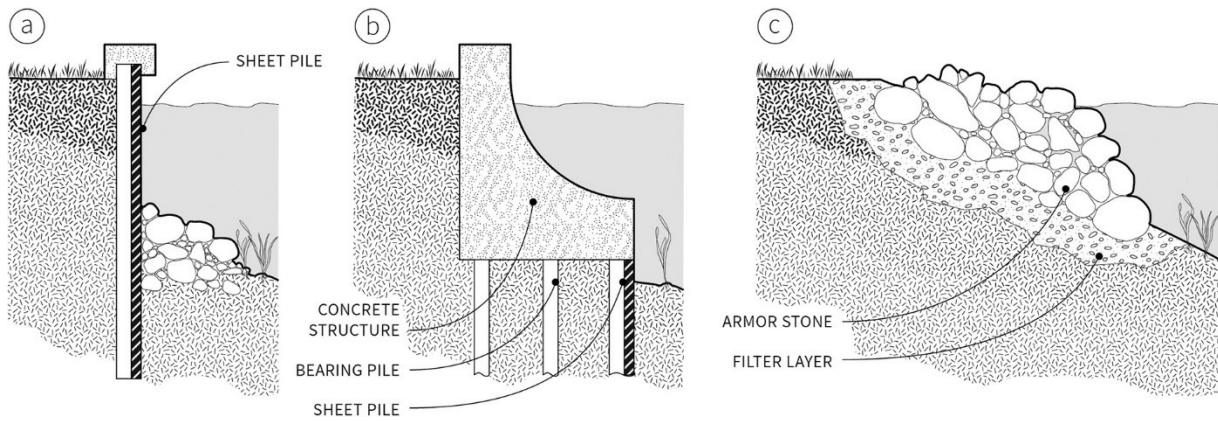


Figure 2.1: Designs for Coastal Protection: a) Vertical Seawall, b) Curved Seawall, c) Riprap (Hosseinzadeh et al 2022)

2.2.2 A Review of Concrete Seawall Designs

Vertical seawalls are appealing in locations where there is limited spaced for construction and when dealing with harsh wave conditions and high surges. The stability of a vertical seawall against lateral forces and sliding relies on their weight and the friction with the underlying surface. However, seawalls in such locations often experiences high wave reflection in the front of the structure, with a reflection coefficient close to unity. This phenomenon leads to an increase in forces exerted on the seawall which results in erosion and scouring at the base (Hosseinzadeh et al. 2022).

The design of curved seawalls serves many purposes, including the reduction of wave overtopping as well as the redirecting of the energy of breaking waves back in a seaward direction (Hosseinzadeh et al. 2022). This curved shape effectively dampens the intensity of wave energy, resulting in lower stress magnitudes. In 2017, Eslami completed a comprehensive failure analysis which indicated that when subjected to dynamic loading, curved seawalls exhibit greater stability and outperform their vertical counterparts. However, it should be noted that in comparison to vertical seawalls, curved seawalls are typical more complex and difficult to design and construct (Hosseinzadeh et al. 2022).

Riprap or rubble mounds are essentially embankments of various materials including concrete blocks. They are notably the most cost-effective seawall design in comparison to vertical and curved seawalls. Furthermore, this type of seawall does not tend to completely collapse when experiencing harsh conditions but instead will only lose partial parts of the system and continue functioning as intended (Hosseinzadeh et al. 2022). Ripraps consist of a porous geometry which

results in greater wave energy dissipation and reduced wave reflection. In cases of high tidal flows, unique types of riprap configuration consisting of interlocking concrete blocks can be utilised to minimise wave run-up, overtopping and scouring at the base of existing seawalls. The use of interlocking blocks provides design flexibility and adaptability in deployment. These riprap designs offer versatility in coastal protection strategies as they can either form the seawall itself or serve as the foundation for other types of seawalls. For example, they can be utilised in front of a vertical seawalls to prevent scouring (Hosseinzadeh et al. 2022).

According to Hosseinzadeh et al. (2022), when it comes to selecting the correct seawall design for locations subjected to high wave surges and harsh wave conditions, the vertical seawall design (Figure 2.1 (a)) is optimal. Due to the vertical face, structure weight and friction created from the underlying surfaces, vertical seawalls are a trusted and stable protective solution that effectively counteracts the horizontal impact forces inflicted from waves and debris (Hosseinzadeh et al. 2022).

2.3 Glass Fibre Reinforced Polymer

2.3.1 General

As per research conducted by Sheikh and Kharal in 2018, glass fibre reinforced polymer (GFRP) bars present a feasible and cost-effective solution to the problem of steel corrosion. This composite material encompasses numerous robust individual glass fibres bonded together with a durable resin, which can be either epoxy or polyester. The resin serves a dual purpose – it protects the fibres from weathering and chemical degradation while also allowing for an even distribution of stresses across all the fibres. When these fibres are securely compressed and bounded by the resin, they yield a strong and rigid material. A study conducted in 2018 by Sheikh and Kharal's involved evaluating the behaviour of GFRP reinforced concrete in flexure, shear, tension, and compression. The study revealed that the fibre composite material has a higher stress capacity than steel and acts linear elastic until failure (Sheikh & Kharal 2018).

Hu and Liu (2010) explain that glass fibres are primarily derived with minor additives from silica sand and are subjected to high-temperature heating until they become molten glass. To form fine strands, this molten glass is then extruded through a mould with smaller apertures ranging from 5 to 24 μm . Once cooled, these strands are wound together to form fibre creel. Pultrusion technology is then commonly used to impregnate fibres with resin to form the GFRP bars (Hu & Liu 2010).

2.3.2 Non-Corrosive Behaviour of GFRP

Fiber composite materials are widely renowned for their resistance to corrosion, a highly favourable feature, especially considering the susceptibility of traditional steel reinforcement to chemical attacks which can result in structural weakening and premature failure. However, as fibre composite technologies are still relatively new, many industry professionals are concerned that the performance and lifespan of fibre composite materials are being overestimated. Such apprehensions have developed due to the fact that many structures that utilise fibre composites have not yet reached the later years of their expected serviceability life. Therefore, the lifespan and durability of fibre composite materials has only been assessed through accelerated degradation testing.

Furthermore, experimental studies have revealed that GFRP bars are not entirely impervious to chemical attacks and weathering. Academic studies have documented GFRP bars exhibiting a sensitivity to alkaline environments, moisture, extreme temperature fluctuations and freeze thaw cycles. Results from an experiment conducted by Yan, Lin, Zhang, Gao and Li (2017) indicate that these climatic conditions have negative impacts on the fibres tensile strength, ultimate strain and modulus of elasticity (Yan et al. 2017). A cover three times the thickness of the reinforcement bar was concluded to be insufficient in protecting the GFRP bars from freeze thaw cycles as failure occurred after 75 cycles while the reinforcements modulus of elasticity was reduced greatly by 26% (Yan et al. 2017).

Additional research by Fergani et al. in 2018 revealed that moisture penetration significantly affects the mechanical properties of GFRP bars. The investigation demonstrated that when specimens were immersed in alkaline solution, moisture is able to permeate through micro-cracks in the protective resin, initiating the dilapidation of certain chemical matrices within the glass fibres, resulting in strength reduction (Fergani et al. 2018). The rate of breakdown was influenced by temperature and alkali concentration. Furthermore, in 2018, Alachek, Reboul and Jurkiewicz's investigation revealed that specimens submerged in water for 10 months exhibited the most pronounced bond degradation, with a considerable reduction of 71% in shear strength.

2.3.3 Modulus of Elasticity

Jabbar and Farid completed an investigation of bending strength and discovered that in contrast to steel bars, GFRP bars displayed a higher strain percentage at initial failure. In other words, the GFRP bars underwent considerably a more significant deflection before failure. This is significant as the design and application of GFRP reinforcement can be controlled by serviceability requirements whereas steel designs are generally governed by ultimate limit states. Furthermore, El-Nemr et al. (2018) confirms that GFRP bars can encounter greater deflections than steel as its modulus of elasticity is approximately 25% less than conventional steel.

Gribniak, Rimkus, Torres and Hui (2018) completed a study that compared the cracking patterns of beams with varying types of GFRP bars with changing stiffness. The study demonstrated that a reduction in the bars modulus of elasticity can result in more substantial and expansive cracking. Results from the investigation also revealed that a decrease in stiffness leads to increased beam deformation and hence greater cracking. This an unfavourable outcome as cracking is the main cause of deterioration in reinforced concrete as it enables moisture to easily invade the concrete. In rigorous cases, this can lead to spalling which can directly expose the reinforcement to environmental influences.

2.3.4 Flexural Performance

A study completed by Jabbar and Farid (2018) applied the mechanical characterisations of GFRP reinforced concrete and compared it with that of steel bars. The investigation revealed that up until the yield point, the steel performs with a linear-elastic relationship, where it continues to deform while maintaining strength. The GFRP resulted in a higher yield strength than the traditional steel, however, unlike the steel, the GFRP bar loses strength at the point of yield (Jabbar & Farid 2018). These behaviour of the GFRP and steel is depicted in Figure 2.2.

Likewise, a study completed by Sadraie et al. (2019) involved undertaking axial tension tests on 8mm diameter steel and GFRP reinforcements and revealed similar results to Jabbar and Farid (2018). As shown in figure Figure 2.3, the steel continues to deform while maintaining strength whereas the GFRP in comparison loses strength at the point of yield.

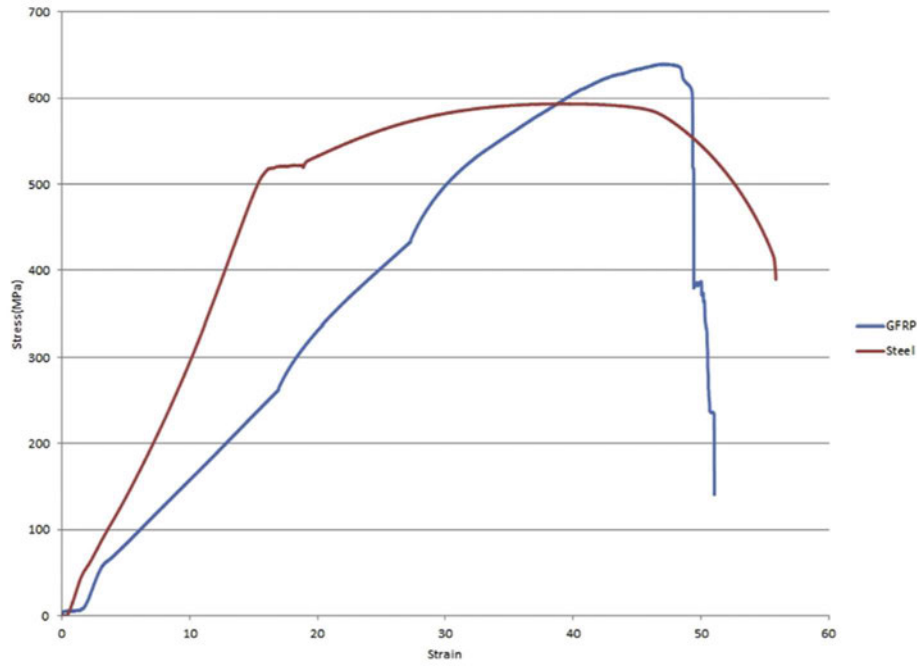


Figure 2.2: Tensile Stress-Strain Curve of GFRP & Steel Bars (Jabbar & Farid 2018)

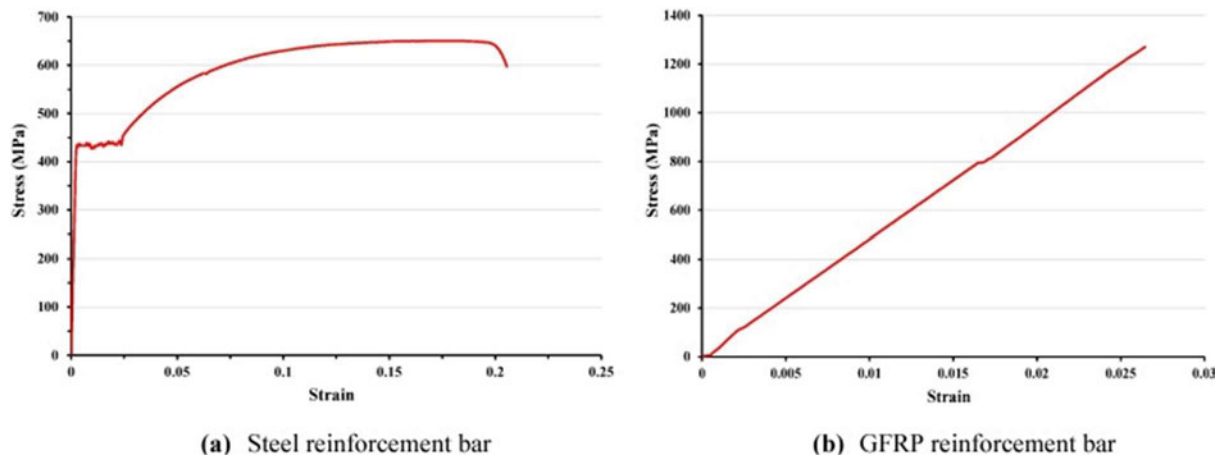


Figure 2.3: Comparison of Axial Tension Results of Steel & GFRP Reinforcement (Sadraie et al. 2019)

In another study, Wang et al. (2022) examined the flexural performance and failure mode of twelve GFRP reinforced beams. The experiment involved exploring various parameters including (1) the reinforcement ratio, (2) the stirrup ratio, (3) prestress level, and (4) shear span ratio. Regarding the influence of the GFRP reinforcement ratio on the flexural performance of the beam, the study concluded that this parameter exhibited a highly significant impact. By increasing the reinforcement ratio, the flexural stiffness of the specimen was increased and caused the failure mode to transition from a GFRP bar rupture to concrete crushing at failure at effectively reduced the ultimate deflection, maximum crack width and strain of the GFRP

bars (Wang et al. 2022). In instances where the specimen failed as a result of GFRP bar rupturing, the reinforcement ratio emerged as a critical component influencing the ultimate load of the specimen. However, the impact of the reinforcement ratio only slightly affected the cracking load (Wang et al. 2022).

2.4 GFRP Reinforcement Standards and Specifications

In reinforced concrete applications exposed to aggressive marine environments, GFRP bars has emerged as a viable alternative to traditional steel bars. In Australia, there is currently no standards or codes regarding the safe design or use of GFRP in reinforced structures. However, the Australian Building and Construction Codes allow the use of international design codes for specific materials.

Codes for the use of fibre reinforced polymer bars in the construction industry have been developed by international institutes such as the American Association of State Highway and Transportation Officials (AASHTO), the American Concrete Institute (ACI) and the Canadian Standards Association (CSA) (Ruiz Emparanza et al. 2017). It is also important to note that currently the Canadian standard CSA S806 Design and Construction of Building Components with Fibre Reinforced Polymers is the most widely accepted standard and is referenced by the Queensland Government in the Department of Transport and Main Roads (TMR) Technical Specification – MRTS271 GFRP Reinforcement.

Similar to steel reinforcement, GFRP bars are offered in varying diameters, ranging from 6 to 36mm. However, unlike steel reinforcement, which exhibits consistent properties across different bar diameters, GFRP bars' longitudinal strength is influenced by size due to the shear lag effect (Bank 2006). For instance, research by Hollaway (2008) demonstrated that when the bar diameter increased from 9.5 to 20mm, the tensile strength of the bar reduced by 40%. As a result, manufacturers are obliged to provide the characteristic strength, stiffness, physical and durability properties for every type of fibre-reinforced polymer bar.

Globally, the specifications of GFRP bars does slightly differ depending on the manufacturer. Below in Table 2.1 is the mechanical properties for American GFRP Bars sourced from Aslan 100 and Table 2.2, is the specifications for the GFRP bars used in this research project sourced from Beyond Materials Group.

Bar Number	Nominal Diameter (mm)	Nominal Area (mm ²)	Tensile Strength (MPa)	Elasticity Modulus (GPa)	Ultimate Strain
2	6	31.67	896	46	1.94%
3	10	71.26	827	46	1.79%
4	13	126.7	785	46	1.64%
5	16	197.9	724	46	1.57%
6	19	285	690	46	1.49%
7	22	387.9	655	46	1.42%
8	25	506.7	620	46	1.34%
9	29	641.3	586	46	1.27%
10	32	791.7	551	46	1.19%

Table 2.1: Mechanical Properties of Aslan 100 GFRP Bars

Bar Diameter (mm)	Nominal Diameter (mm)	Nominal Area (mm ²)	Tensile Strength (MPa)	Elasticity Modulus (GPa)	Ultimate Strain
8	7.5	44	1410.5 (41.3)	63.5 (0.9)	> 1.5%
10	9.5	71	1340.5 (37.3)	63 (1.1)	> 1.5%
13	12.7	127	1301.3 (20.4)	63 (0.5)	> 1.5%

Table 2.2: Mechanical Properties of Beyond Materials Group GFRP Bars

2.5 Effect of Bar Diameter on Physical, Mechanical and Durability Properties

The diameter of GFRP bars used as internal reinforcement in concrete structures are not currently considered within any standards or specifications. However, a study undertaken by Benmokrane et al. (2017) investigates the effects of bar diameter on the physical and mechanical properties as well as the durability of GFRP reinforcing bars conditioned for three months at 60°C in an alkaline solution simulating a concrete environment. Five diameters (nominal diameters of 9.5, 12.7, 15.9, 19.1 and 25.4 mm) were considered and the bar properties were assessed before and after conditioning. The results revealed that the bar size had no considerable influence on the bar's physical properties, except for water absorption (Benmokrane et al. 2017). The smaller diameter bars were found to have higher water absorption than the larger ones with the same length because of their higher surface area to volume ratios. In regard to the unconditioned bars, due to the efficient stress transfer from the bar surface to the centre, the tensile strength and modulus were not notably affected by bar diameter. Conversely, results revealed that there was a size effect for interlaminar shear strength and flexural strength due to larger diameter bars having a higher probability of defects therefore causing a lower interlaminar shear strength and flexural strength in comparison to smaller diameter bars. Equally, the conditioning in the alkaline solution had a greater negative impact on the tensile strength of the larger bars than on the smaller ones. Scanning electron microscope (SEM) observations and Fourier Transform Infrared Spectroscopy (FTIR) analysis exposed that the degradation remained at the surface of all the conditioned samples. Nonetheless, there were only subtle differences concerning the physical and mechanical properties of the GFRP bars of varying diameters. This suggests that the current conditions in standards that do not relate strength retention limit to bar size are acceptable (Benmokrane et al. 2017).

2.6 GFRP Bars as Reinforcement in Concrete Structures

In accordance with the Australian Standard for Concrete Structures (AS 3600), an under-reinforced section is considered desirable when designing a traditional reinforced concrete section as the objective is to fully utilise the strength of the steel reinforcement before reaching failure. To ensure that the steel bars yield before undergoing a ductile failure, a special consideration is given to the neutral axis parameter (k_u). A ductile failure is more favourable than a brittle failure as it aids engineers in repairing structures before failure occurs as the bars will deflect greatly before completely failing. Therefore, to ensure yielding, concrete sections must be designed so that k_u which is a ratio of the ultimate strength under any combination of bending and compression between the neutral axis depth and the most extreme compressive fibre is less than 0.545 (AS 3600). Exceeding this threshold would classify the section as over-reinforced, posing the risk of sudden failure due to concrete crushing. For an even more optimal design, aiming for a k_u value below 0.36 is advisable (AS 3600). When this criterion is met, it results in a balanced condition where the design will fail gradually due to both concrete crushing and the steel bars yielding. This is a desirable design outcome as it ensures that the section has the highest possible capacity.

However, in terms of sections reinforced with GFRP bars, the conventional design principles cannot be directly applied due to some key parameters. Achieving a balanced failed criterion, as with steel reinforcement, is not feasible because GFRP bars do not undergo yielding like steel; they exhibit linear elasticity until immediate failure. Due to their modulus of elasticity, GFRP reinforced sections are typically over-reinforced and therefore fail via concrete crushing. Khorramian and Sadeghian (2017) conducted an experiment evaluating the performance of short concrete columns reinforced with GFRP bars. The study revealed that each test failed primarily due to concrete crushing, while the GFRP bars displayed no indication of failing at peak load. This was corroborated by strain gauge data, which indicated that the GFRP bars only reached 50% of their predicted strain capacity (Khorramian & Sadeghian 2017).

Further investigations on GFRP-reinforced beams conducted by Gu, Yu and Wu (2016) identified a number of factors which clearly influenced the performance of GFRP reinforcement. The key findings include:

- Small bar diameters are preferable, as increasing the bar diameter reduced the peak bond strength.
- The shear strength of GFRP bars typically amounts to approximately 20% of its tensile strength.
- GFRP reinforced specimens achieve about 60% of the bond strength compared to steel-reinforced specimens.
- As the same reinforcement ratio and geometric size, GFRP and steel reinforced beams have similar bearing capacities. However, GFRP reinforced beams exhibit poorer crack control.

In 2016, Goldston et al. investigated the behaviour of concrete beams reinforced with GFRP bars. A total of twelve GFRP reinforced beams were designed and tested where six were subjected to static loading and the other remaining six were subjected to impact loading using a drop hammer machine. The two key parameters explored within this investigation was the reinforcement ratio, ranging from 0.5% to 2.0% and the compressive strength of concrete, set at 40 and 80 MPa. Results revealed that increasing both the reinforcement ratio and the concrete compressive strength led to an increase in post cracking stiffness and bending moment capacity in the beams (Goldston et al. 2016). Another noteworthy conclusion from this study is that the reinforcement ratio displayed a more significant influence on the energy absorption capacity of the beams in comparison to the compressive strength of the concrete. This discrepancy can be attributed to the GFRP bar's superior deformation resistant properties when contrasted with concrete. Under impact conditions, this heightened resistance provided the beam's ability to withstand additional loading (Goldston et al. 2016).

Furthermore, a comprehensive study conducted by Maranan et al, (2015, 2017, 2018) demonstrated that GFRP reinforced geopolymer concrete beams with a similar reinforcement ratio, resulted in a 23% increase in flexural strength and also an 85% increase in deflection in comparison to steel reinforced geopolymer concrete counter parts. This difference in performance can be attributed to the GFRP bar's greater tensile strength but lower elastic modulus in contrast to steel bars. The investigation also revealed that an increase in the reinforcement ratio improved the cracking behaviour of the beams (Maranan et al. 2019).

2.7 Steel, GFRP & FRP Reinforced Concrete Slab Subjected to Impact Loading

Othman et al. (2016) evaluated the dynamic performance of steel reinforced concrete slabs under low velocity impact loading. The study involved a total of 10 impact tests on five high strength concrete (HSC) plates (two tests per specimen). The process of the investigation involved dropping a 475kg steel weight at the mid-point of the specimens from a constant height of 4.15m. The paper evaluated two parameters namely: altering the steel reinforcement ratio (1%, 2% & 3%) and the steel reinforcement configuration (single or double mesh). Results from the study indicated that the crack pattern and mechanism of failure were found to be more dependent on the reinforcement arrangement than on the reinforcement ratio. This is because the arrangement of reinforcement helps control the formation and propagation of cracks. When a load is applied, tensile stresses develop, and cracks can initiate in areas of high stress. Therefore, the arrangement of reinforcement can control or confine the cracks to specific areas. It helps distribute the applied load more evenly, therefore preventing the formation of large uncontrolled cracks. In relation to the mechanism of failure, reinforcement bar provides ductility to concrete, allowing it to deform and absorb energy before reaching failure. In contrast, a weak reinforcement arrangement can result in sudden and brittle failure as there are limited warning signs or deformation prior to collapse. It was also noted that there was no significant effect on peak displacement when increasing the steel reinforcement ratio for single reinforced plates. Conversely, the residual displacement was found to be inversely proportional to the reinforcement ratio (Othman & Marzouk 2016).

In 2022, Salih et al. conducted an experimental investigation into the behaviour of one-way GFRP reinforced concrete slabs under an impact load and compared it to the behaviour of a one-way steel reinforced concrete slab. The experiment involved the casting of six 4000mm x 1000mm x 180mm concrete slabs and subjecting the test specimens at mid-point to a drop weight of 7kg from two different heights, one meter and two meters. Results from the investigation concluded that the strain of the GFRP reinforced slabs was 25% less than the steel reinforced slabs and the time interval was also 37.5%. The study ultimately established that the behaviour of the GFRP reinforced concrete slabs performed a lot better than the slabs reinforced with steel under impact loading conditions notably as the lower strain in GFRP reinforced slabs signifies improved crack control and potential enhanced durability of the structure (Salih et al. 2022).

Xiao et al. (2017) completed an experimental and numerical investigation into the behaviour of steel reinforced concrete slabs subjected to low velocity impact loads. This study revealed that by increasing the concrete strength, slab thickness and the diameter of the impacted area, the energy capacity can be significantly increased, whereas the effect of adjusting the ratio of steel reinforcement was limited (Xiao et al. 2017). This is because higher concrete strength allows the material to withstand greater impact forces without experiencing failure by increasing the load-bearing capacity of the slab. Thicker slabs have a larger volume of concrete providing greater resistance to impact forces as the additional material helps absorb and distribute energy over a larger area. Furthermore, increasing the diameter of the impact area means the forces are distributed over a larger surface area therefore reducing the localised stress (Xiao et al. 2017).

In another study, Sadraie et al. (2019) completed an experimental and numerical investigation the dynamic behaviour of steel and GFRP reinforced concrete slabs to impact load with low velocity. The investigation centred its critical findings on evaluating the impact response of bar type (steel or GFRP), reinforcement ratio and arrangement (single or double mesh), concrete strength (30MPa and 60MPa), and slab thickness. Fifteen 1000 x 1000mm concrete slabs consisting of the varying testing parameters were subjected to drop weight impact loads using a 105kg cone frustum headed projectile released from a height of 2.5m. These slabs included two 100mm thick steel reinforced slabs, five 75mm thick steel reinforced slabs, two 75mm thick plain slabs, and six 75mm thick GFRP reinforced concrete slabs. The strain-time, displacement-time, and the acceleration-time responses were obtained and evaluated. Other result responses investigated were the fracture formations and failure mechanism of the test slabs. The study also involved the use of LS-DYNA explicit software to complete a finite element analyses and simulation of the specimens.

The experimental tests and numerical simulations performed by Sadraie et al. (2019) provided numerous results and conclusions regarding the impact response of reinforced slabs. Results indicated that slabs reinforced with either steel bars or GFRP bars performed well in resisting dynamic impact loads. However, in some cases the GFRP reinforced slabs provided slightly less resistance than the steel reinforced slabs (Sadraie et al. 2019). This could be pinpointed to the difference in material properties between steel and GFRP bars. Steel reinforcement typically exhibits higher stiffness and strength which may contribute to a slight superior performance in some cases (Sadraie et al. 2019). Furthermore, specimens reinforced with steel measured lower displacement values than specimens reinforced with GFRP, though it was

concluded that similar or even better behaviour results could be achieved with relatively higher amounts of GFRP than steel bars. It was found that there was a decrease in maximum displacement when there was an increase in reinforcement ratio and the use of double reinforcement (Sadraie et al. 2019). The study went on to conclude that the using GFRP instead of steel as reinforcement lead to an increase in crack development and scabbing mass. However, these characteristics were theorised to improve with a higher consumption of GFRP bars. It was also observed that the weight of concrete debris exhibited variations influenced by both the reinforcement ratio and strength of concrete. Additionally, increasing the reinforcement ratio and concrete strength provided more stiffness and rigidity (Sadraie et al. 2019). Finally, the Sadraie et al. (2019) concluded that improved performance can be achieved by adjusting the amount and arrange of GFRP, which considering the corrosion resistant nature of this material, earns GFRP as an appropriate selection of reinforcement material.

Ramakrishnan. K et al. (2019) studied the effect of impact testing on concrete slabs reinforced with Basalt Fibre Reinforced Polymer (BFRP) bars. In this study, slabs of 550mm x 550mm x 50mm were casted with varying BFRP reinforcement configurations consisting of different bar spacings. The study also incorporated a control slab consisting of steel reinforcement at 75mm centres. The impact testing was completed using a drop weight of 3.75kg from a height of 1.2m. The aim of this experiment was to determine the impact strength of the slabs through the number of drops required to create the first crack and ultimate failure of the slabs. The results of the investigation showed that due to the low ductile nature of the BFRP bars, the slabs consisting of this reinforcement resulted in more cracks than the slabs reinforced with steel bars. However, the study did conclude that the BFRP bars are a more desirable alternative solution than traditional steel reinforcement as they resulted in a higher ultimate crack resistance and crack resistance ratio (Ramakrishnan & Vinodhini 2019).

Said and Mouwainea (2022) completed an investigation evaluating the high-mass, low velocity impact behaviour of reinforced concrete slabs. The study involved testing six sample two-way slabs and validating the experimental data with numerical modelling. The aim was to analyse the effects of different reinforcement ratios and compressive strengths of concrete on the dynamic response and behaviour of steel reinforced concrete slabs. The key findings from the study are as follows:

- By increasing the longitudinal reinforcement ratio did not affect the impact responses of the slabs.
- It was observed that the penetration depth and scabbing area decreased as the compressive strength and reinforcement ratio increased.
- All test samples after the first impact event displayed circumferential cracks as a sign of punching failure.
- The concrete slab with the largest reinforcement ratio was the most resistant to local damage.

2.8 Local and Global Response

The assessment of failure modes in reinforced concrete structures subjected to impact loading can be determined both locally and globally. Bangash (1993) classified this particular phenomenon as follows:

- (a) Penetration: This pertains to the measurement of the depth of the resulting crater in the target material (Figure 2.4 (a)).
- (b) Perforation: This entails the complete penetration of the target material by the impacting object, either with or without exit velocity (Figure 2.4 (b)).
- (c) Scabbing: This describes the expulsion of fragments from the opposite face of the target material upon impact (Figure 2.4 (c)).
- (d) Spalling: This denotes the expulsion of material from the impacted face of the target (Figure 2.4 (d)).
- (e) Global Response: This refers to the structural behaviour involving global bending, shear, and membrane action, as well as the changing mode of failure in concrete slabs (Figure 2.4 (e)).

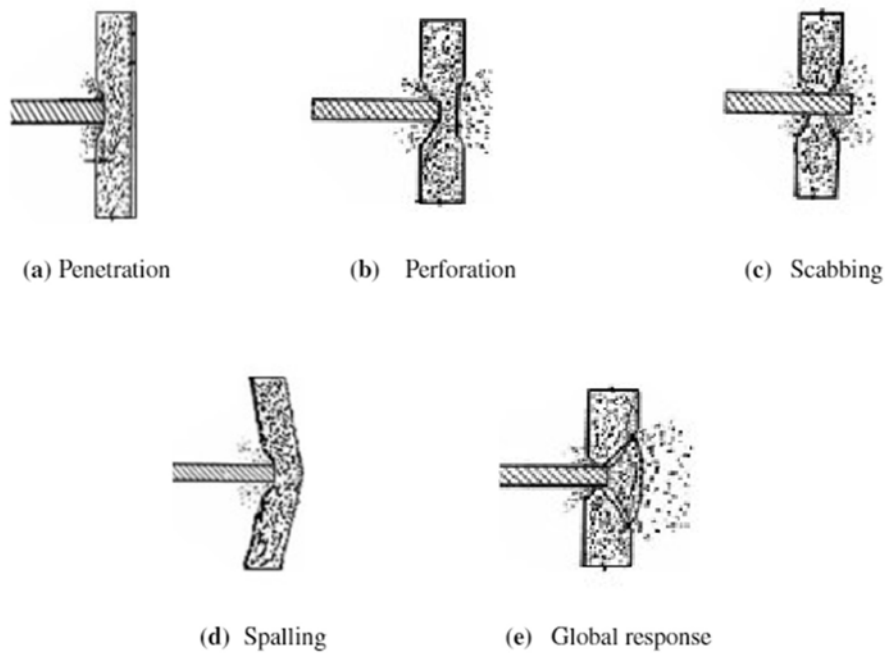


Figure 2.4: Different Forms of Impact Damage (Bangash 1993)

2.9 Failure Mode of Steel Reinforced Concrete Slabs Subjected to Impact Loading

Research indicates that there are three primary failure modes of steel reinforced concrete slabs subjected to impact loading. They are classified as follows:

- Flexural mode: as shown in Figure 2.5 below, this failure mode involves cracking in the tensile zone and yielding steel (Tahmasebina 2011).



Figure 2.5: Flexural Mode

- Ductile Shear: this failure mode entails cracking in the tensile zone, crushing in the compressive region and yielding steel (Figure 2.6) (Tahmasebina 2011).

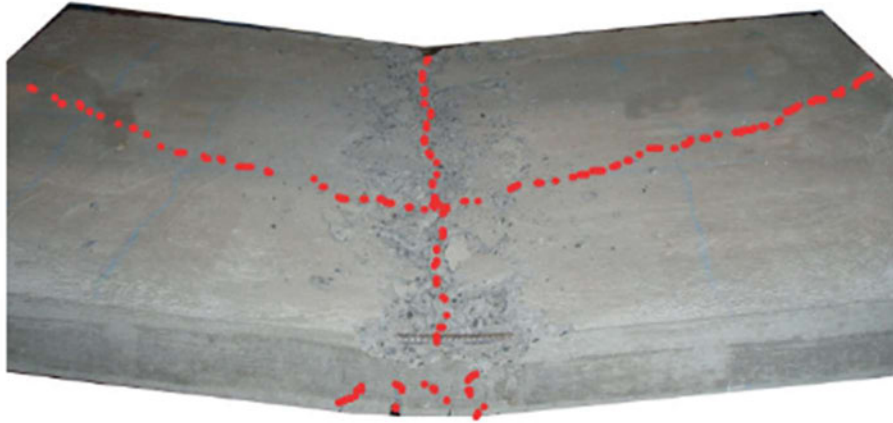


Figure 2.6: Ductile Shear

- Shear Failure: as demonstrated in Figure 2.7 below, this concept involves shear failure as 45° angles (Tahmasebina 2011).



Figure 2.7: Shear Failure

Satio et al. (1995) conducted both experimental and numerical investigations to assess the loading capacities, deformations, and failure patterns of different types of reinforced concrete slabs when exposed to varying rates of applied loads. The study revealed a significant correlation between the mode of failure and the rate at which the load was applied. The comparison of results from both the experimental and numerical testing is shown in the Figure 2.8.

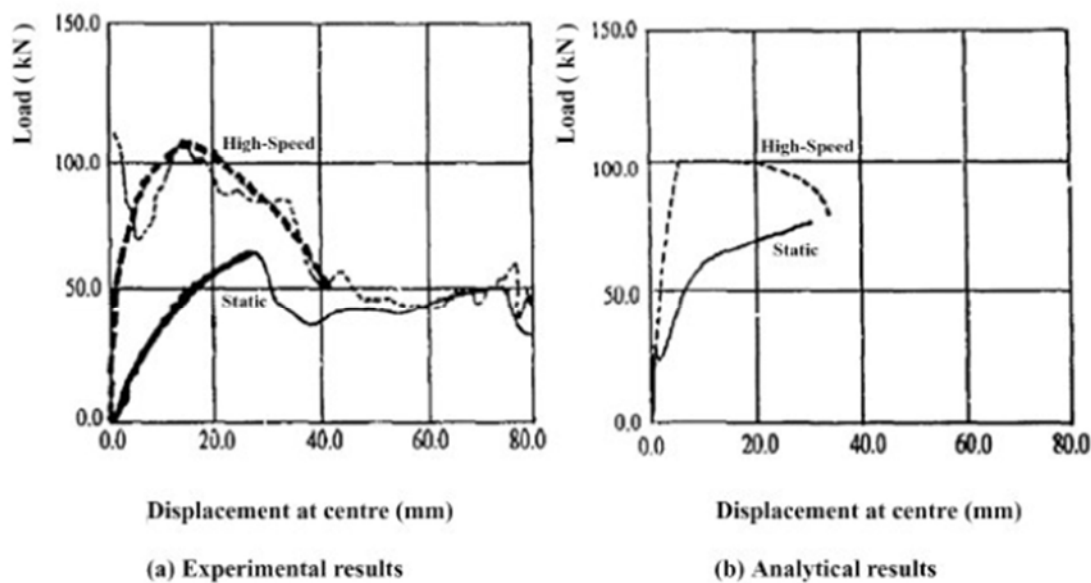


Figure 2.8: Experimental and Analytical Load -Displacement Figures (Satio et al. 1995)

The study also conducted an investigation into the application of concentrated loads to the surfaces of reinforced slabs under static, low, and high rates. The experiment revealed that as long as the rate increased, then the deformation and failure mode changed from flexural to punching shear mode (Satio et al. 1995).

Yankelevsky (1996) undertook a theoretical study with a primary focus on perforation and shear punching. The investigation encompassed two key phases which outlined the progression of a target being impacted and it leading to the development of punching shear as visualised in Figure 2.9.

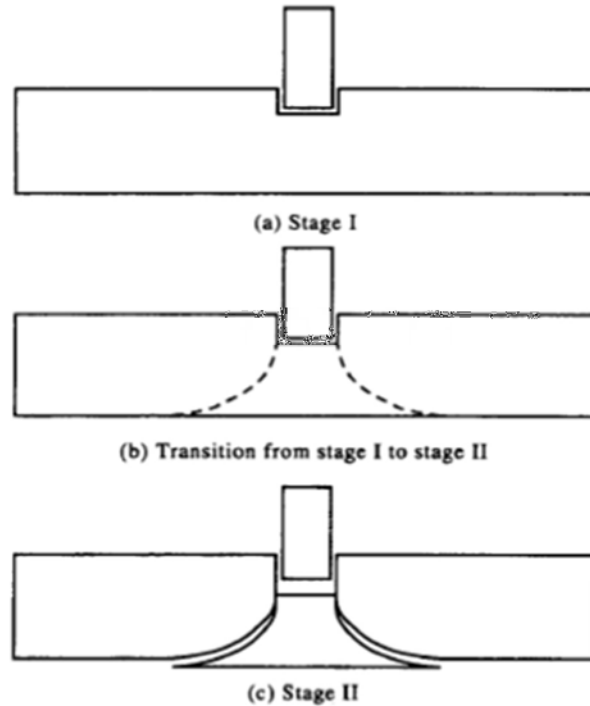


Figure 2.9: Perforation and Shear Punching Transition (Yankelevsky 1997)

Delhomme et al. (2005) emphasised the significance of an observation regarding the damage process in a slab subjected to an impact load. The study recognised this as a critical parameter capable of influencing the mode of failure under impact loading conditions, and they categorised it into distinct modes as follows:

- Initial cracking or fractures
- Materials of the two colliding elements
- Velocity of the striker
- Rigidity of structure
- Incidence angle of the colliding elements
- Shape of the dropped hammer

It should be noted that this categorisation is not solely derived from the impact loading itself. Determining realistic impact failure modes in reinforced slabs exposed to impact loading is a complex endeavour, demanding individual investigation. Therefore, it is suggested that a combination of impact and static analyses be considered as real-world scenarios might involve a mix of failure modes within each designated slab rather than conforming to a single mode (Tahmasebina 2011).

2.10 Research Gap

There are numerous empirical studies evaluating the performance of GFRP bar reinforcement in concrete elements such as beams, columns, and railway sleepers. Similarly, there is a substantial amount of research investigating different parameters of steel reinforcement subjected to impact loads. However, there is a lack of research specifically evaluating the performance of different GFRP bar diameters under impact loading conditions. This research investigation aims to provide insight into the performance of different GFRP bar diameters in seawalls when subjected to high impact forces such as powerful waves and boat collisions during extreme weather events.

The focus on bar diameter as a parameter of investigation aims to provide insight into the optimal design of seawalls as it directly affects certain aspects such as load bearing capacity, crack propagation, energy absorption and dynamic response. The interplay between bar diameter and these key factors plays a critical role in determining overall performance and structural integrity of concrete slabs subjected to impact loading conditions. This investigation will lead to further work in refining the design of seawalls by investigating other various parameters such as GFRP reinforcement quantity, configuration, and different concrete strengths, and if found suitable, further research into other FRP reinforcement options for use in similar applications.

Chapter 3 Preliminary Drop Weight Testing

3.1 Chapter Overview

This chapter pertains to the initial phase of this research paper, wherein various drop weight heights are subjected to preliminary testing. The primary aim of this initial testing phase is to:

- To refine the experimental methodology to ensure efficiency when completing the official testing phase.
- To ensure all systems are working including the DIC, strain gauges, force sensors and accelerometers.
- To investigate the effectiveness of the test set-up, transitioning it from a theoretical construct to a practical realisation.
- To validate the drop height and its effectiveness in damaging the test samples in preparation for the official testing.

3.2 Specimen Details

A rectangular concrete slab from the UniSQ Centre for Future Materials (CFM) building was used as the preliminary test sample. The slab consisted of 12.7mm diameter GFRP bars with 30mm of cover. The internal reinforcement configuration is depicted in Figure 3.1.

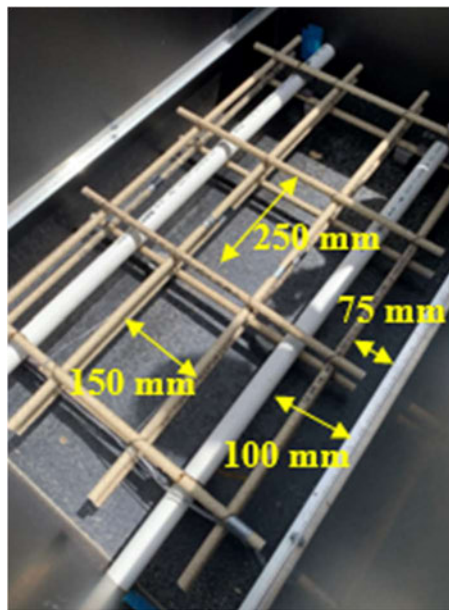


Figure 3.1: Test Slab Internal Reinforcement Configuration

3.3 Experiment Set-up

Table X summarises the key set-up components required to complete the preliminary testing. Figure 3.2 depicts the theoretical test setup which was developed as an initial guide to setting up the experiment. For comparison, Figure 3.3 is the actual preliminary test setup.

Set-up Components	
Test Frame	Accelerometers
Crane	Strain Gauges
300kg Drop Hammer	Force Sensors
Computer	Force Sensor Protective Plate
DIC Device	Lifting Straps
Data Logger	Safety Protection Screens

Table 3.1: Set-up Components for Preliminary Testing

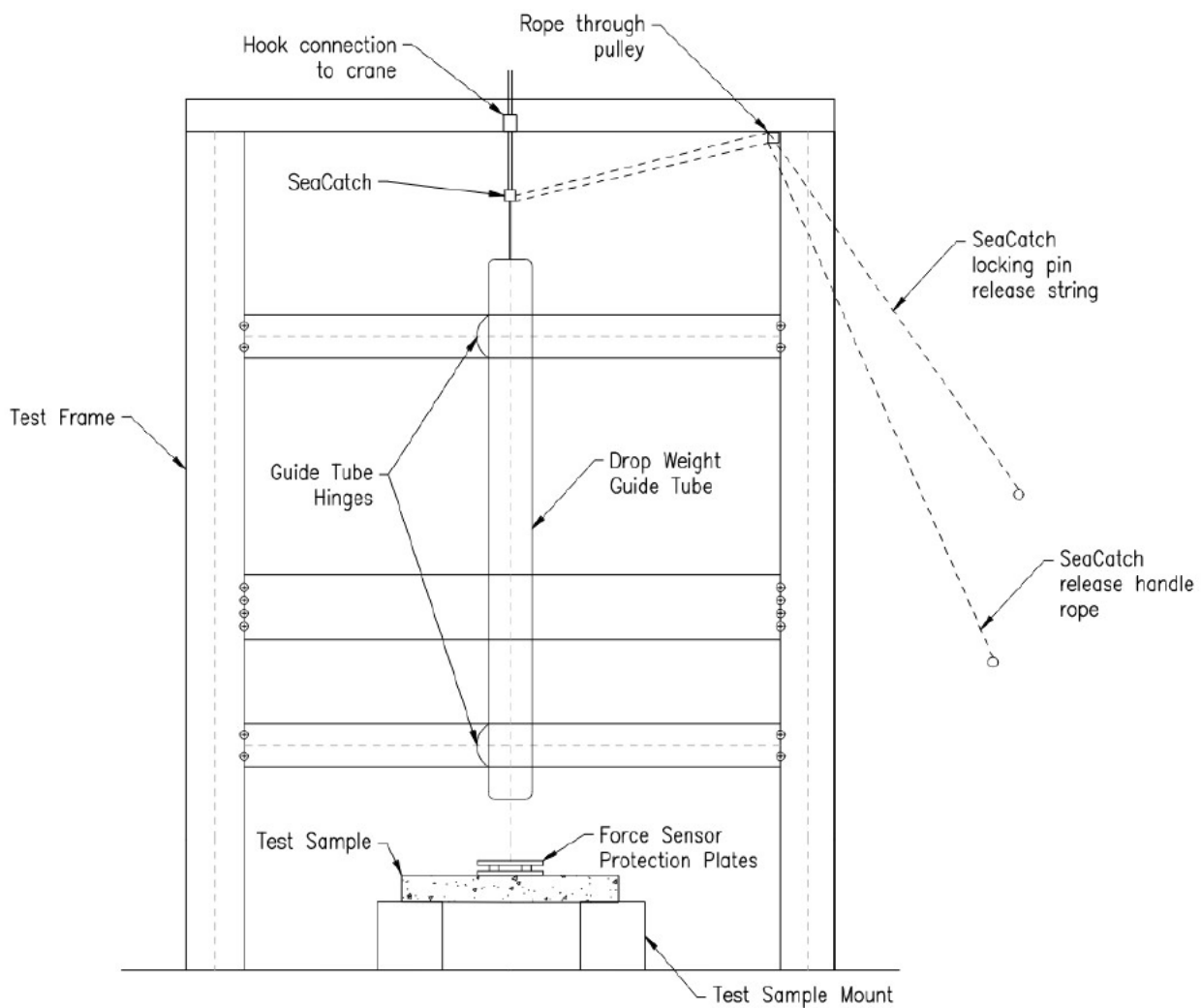


Figure 3.2: Theoretical Test Setup



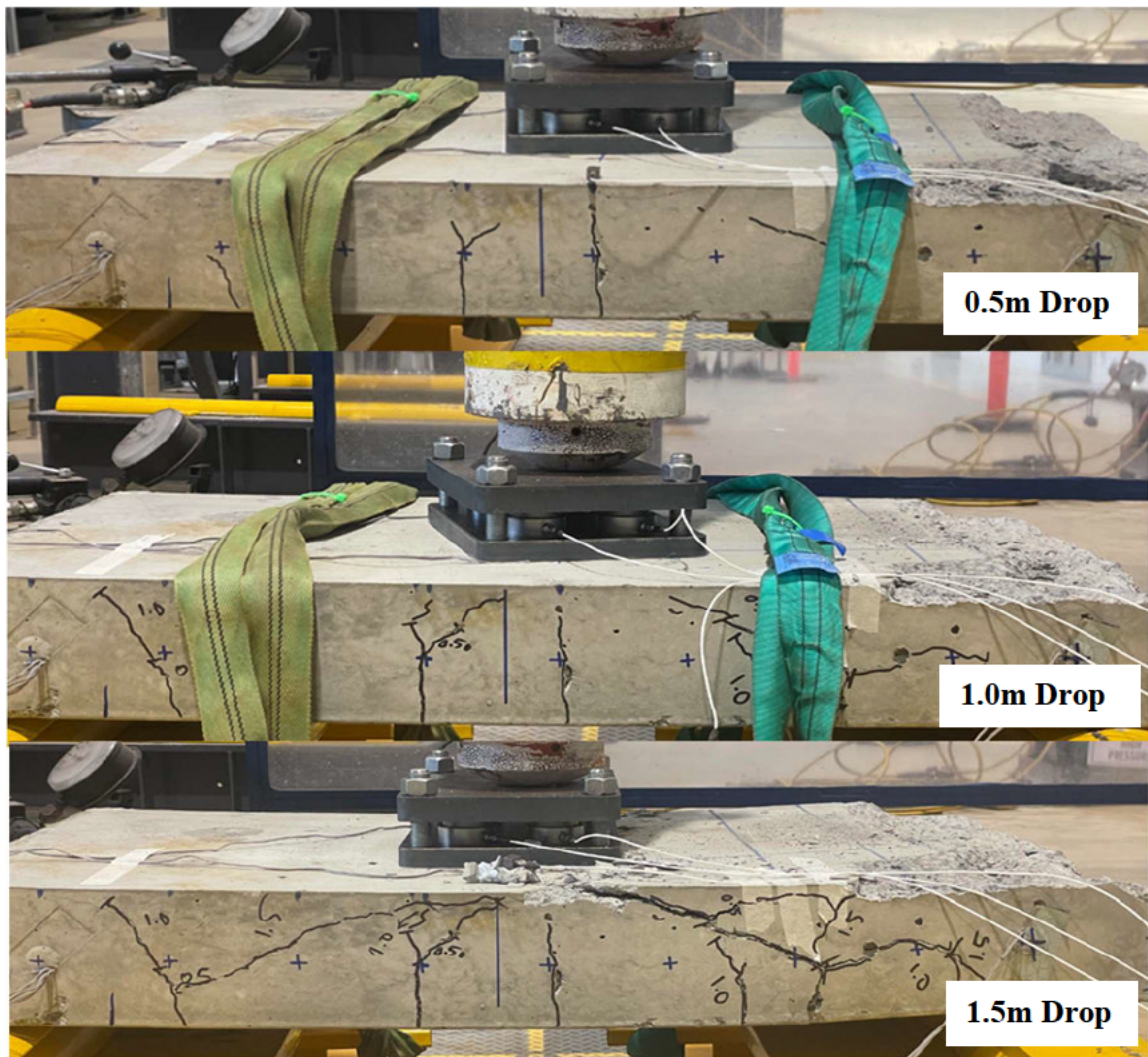
Figure 3.3: Preliminary Test Setup

3.4 Test Methodology

The test specimen was placed centrally under the 300kg drop hammer and was strapped down on either side using lifting straps. All necessary recording data was set up including safety screens to protect all personnel involved in the experiment and devices such as computers. The actual process of testing involved repeatedly dropping the hammer from three different heights including 0.5m, 1m and 1.5m onto the test sample. Upon completion of the drops, the slabs were examined, and observations were recorded.

3.5 Failure Mode Observations

Non-destructive testing observations were completed to evaluate the response of the concrete slab under the impact of a drop weight from three different heights. As illustrated in Figure 3.4, the slab displayed minor tensile cracking following the impact of the 0.5m drop. Subsequent to the 1.0m drop, a notable increase in tensile cracking was observed, accompanied by slight indications of shear failure. Upon experiencing the 1.5m drop, the slab displayed extensive cracking within the tensile zone, crushing in the compressive region, and obvious deformation, indicating the yielding of the reinforcement. Closer scrutiny revealed apparent spalling on the top face. After the drop-test was completed, the slab was raised for removal and a thorough examination of the bottom face was conducted which revealed signs of punching shear and localised failure (Figure 3.5).



3.5 Learnings

Several critical insights were yielded from the preliminary testing phase that should be considered in the upcoming impact testing. Firstly, it was made evident that a sufficient allocation of time is required to complete all phases of the experiment. This includes the initial set up time, precise placement of the slabs using the crane, the execution of the impact testing and the subsequent removal of the used specimens, along with the resetting of equipment in readiness for subsequent testing iterations.

Another notable constraint identified pertains to the availability of technical officers to complete the experiment, this has resulted in the official testing to be complete over a two-week period.

During this initial investigation phase, it was identified that the use of laser technology was required to assist in the precise positioning of the drop weight at a predetermined distance over the test sample, emphasising the importance of correct measuring techniques.

Other learnings from this experiment included the necessity to possibly investigate in alternative adhesive options to attach the accelerometers to the concrete slab face, aiming to enhance the quality and reliability of the sensor attachment. Furthermore, this leads to the identification of ensuring the proper attachment of the strain gages to the top of the slab face, as during the 1.0m drop height phase, an external strain gage was damaged and could no longer record data.

In terms of selecting a drop height suitable for the official testing, it was resolved to utilise the maximum height permissible by the testing frame, which amounts to two meters. The aim is to attain precise and unambiguous results to discern the optimal performance among various bar diameters during the official impact experiment.

Lastly, a structured drop weight release protocol was devised, whereby each individual responsible for releasing the safety pin and initiating the release of the Seacatch verbally declared the completion of their respective tasks. This procedural measure was implemented not only due to safety factors but to also ensure the synchronisation of testing initiation among all personnel involved and to facilitate successful data recording.

The preliminary testing phase is a critical component as it underscores the importance of accurate planning, technical proficiency, and precise instrumentation in the upcoming impact testing. Taking into consideration these learnings will help successfully execute the impact testing.

3.6 Expected Outcomes

Based on foundational structural engineering principles, academic research and the preliminary testing, the following outcomes are anticipated for the official impact test:

- Samples reinforced with larger GFRP bars will provide higher tensile and flexural strength. Therefore, this increase in strength will allow them to withstand impact forces more effectively than slabs reinforced with bars with smaller diameters.
- When subjected to an impact load, larger diameter GFRP bars have a greater capacity to dissipate energy which results in reducing the severity of deformation and cracking in the concrete slab.
- Specimens reinforced with larger diameter GFRP bars will result in a more even distribution of forces and a lower risk of localised failure. This is because the applied loads will be distributed over a larger area, therefore reducing the concentration of stress at any one point in the concrete.
- Based on observations from the preliminary testing, the failure modes and cracking patterns of the test specimens will generally involve tensile cracking, shear cracking and punching shear.
- Although a more brittle material than steel, the GFRP is anticipated to act in a ductile manner and therefore no spalling or perforation is expected. Furthermore, the test set-up only allows for a maximum height drop of 2m and the experiment will be conducted under controlled conditions. This set-up design will ensure that failure modes remain within an acceptable range.

Chapter 4 Official Impact Testing

4.1 Chapter Overview

This chapter involves completing the official impact testing involving the three concrete slabs with varying diameters. Data will be collected and critically analysed using simple mathematical and structural principles. Any significant findings will then be discussed.

4.2 Safety Considerations

Every organisation in Queensland is obliged to comply with the Work Health and Safety Act 2011. This legislation underscores the fundamental principle that every individual has the right to go home at the end of the day in the same condition as they arrived. Therefore, students at the University of Southern Queensland are required to complete a risk assessment for all experimental activities before being granted permission to use the university facilities and equipment. All participants are also required to undergo a formal laboratory site safety induction with a certified technical officer before any testing procedures can commence.

A risk assessment was employed for the preparation and execution of this experiment and was submitted to the university's online safety risk management system. This undergraduate research project was completed as part of a larger research project for PhD student, Ezgi Bal Yetim. Therefore, the risk assessment for this project falls within the risk assessment completed for the overarching research project which can be found in Appendix D.

4.3 Materials

4.3.1 Specimen Details

Three slab specimens were designed for the experiment. All three specimens were casted with 50MPa concrete and have the dimensions of 1000mm x 1000mm x 125mm. The three specimens were reinforced with GFRP bars with the diameters of 8mm, 10mm and 13mm. The typical reinforcement configuration of the slabs involved 20 bars with equal spacing and 25mm of cover was provided for the reinforcement on the side faces on the concrete slab. The internal configurations of the specimens can be found in Appendix C.

Specimen	Reinforcement Type	Bar Diameter (mm)	Number of Bars	Cover (mm)	Concrete Strength (MPa)	Comments
S1	GFRP	8	20	54.5	50	Increasing Bar Diameter
S2	GFRP	10	20	52.5	50	
S3	GFRP	13	20	49.5	50	

Table 4.1: Overview of Specimen Details

4.1.3 Specimen Preparation

The concrete slabs to be evaluated in this research project were prepared and casted by Beyond Materials Group (refer to Figure 4.1). The configuration of each specimen began with first setting up the formwork and arranging each specimen with the correct reinforcement as per the details specified in Table 4.1. Four strain gauges were then attached to the reinforcement bars using adhesive. Once in position, to protect the gauges from moisture and aggregates within the cement mixture, each sensor was wrapped with tape. Concrete was then poured into each mould and was thoroughly vibrated to expel any trapped air and to optimise the density of the concrete. To achieve a finishing smooth and level surface, the cement was hand screeded. The slabs were then left for 28 days to achieve the design strength.



Figure 4.1: Slab Preparation at Beyond Materials Group

4.2 Experiment Set Up

Table 4.2 summaries the key set up components required to complete the official impact testing.

Set-up Components	
Test Frame	Accelerometers
Crane	Strain Gauges
300kg Drop Hammer	Force Sensors
Computer	Force Sensor Protective Plate
DIC Device	Lifting Straps
Data Logger	Safety Protection Screens

Table 4.2: Set-up Components for Official Testing

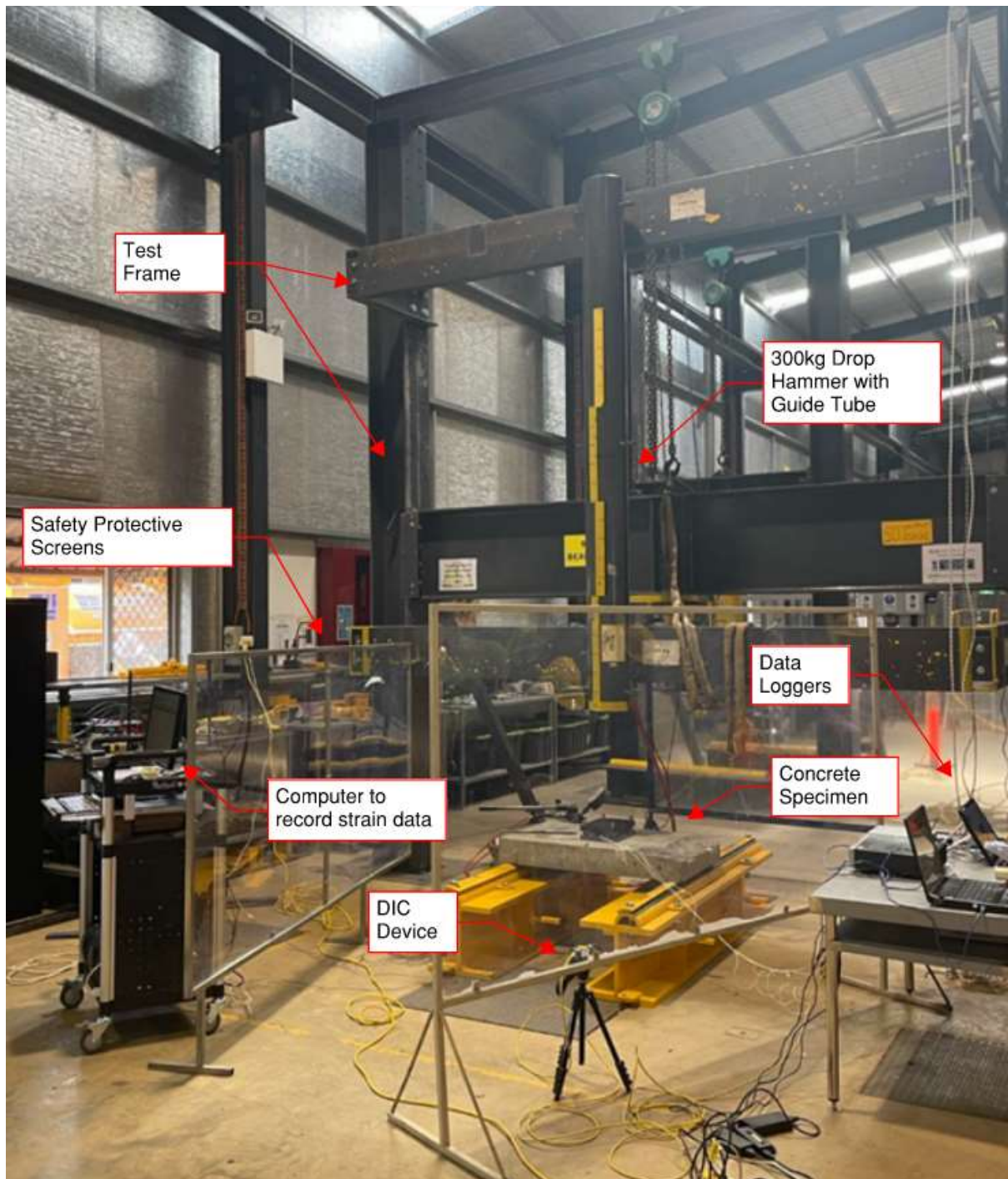


Figure 4.2: Official Testing Setup

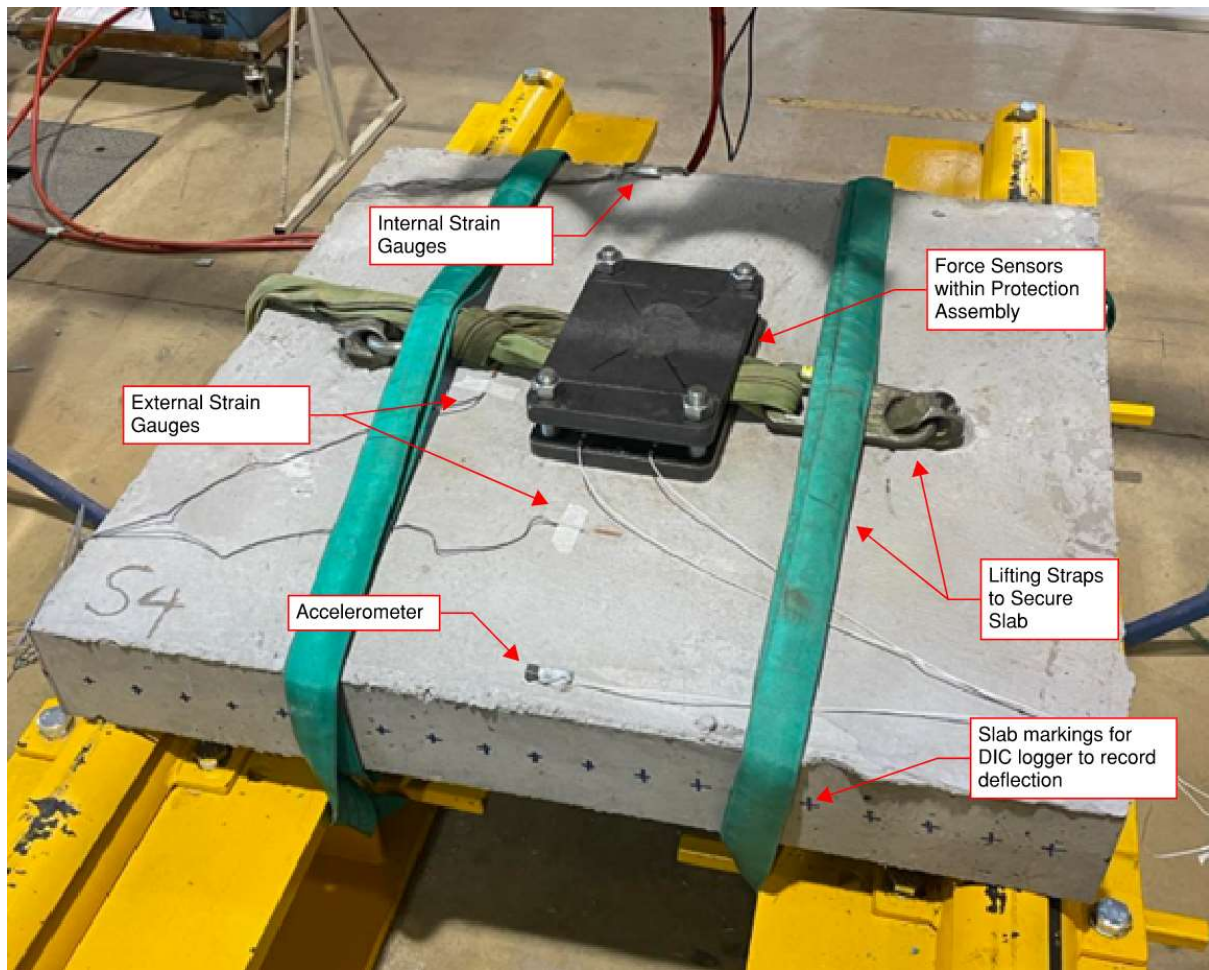


Figure 4.3: Slab Recording Equipment Setup

4.2.1 Accelerometers

Accelerometers are electromechanical mechanisms that measure acceleration. They are utilized in various applications to determine the rate of acceleration experienced by an object in motion.

To record the acceleration of the drop hammer, one accelerometer was attached using beeswax to the top face of the slab as demonstrated in Figure 4.3. Ideally, super glue would have been the best option for attaching the accelerometer to the slab, however the device was required to be reused for all test samples.

4.2.2 Strain Gauges

Strain gauges are specific sensors that are utilised to measure and quantify the strain for deformation of an object when it experiences an external force. When this object is subjected to deformation, the strain gauge records this information by measuring the resulting changes in electrical resistance. They are commonly employed to evaluate the mechanical performance as strain data is often utilised to predict ultimate material failure.

Four strain gauges were attached to the internal reinforcement before the slabs were casted (Figure 4.4). Another two strain gauges were attached using super glue to the compression side of the concrete slab as illustrated in Figure 4.3. The aim of the internal strain gauges was to assess the strain behaviour of the reinforcement when subjected to the impact load whereas the external devices were employed to assess the strain behaviour on the compressive side of the concrete specimens.

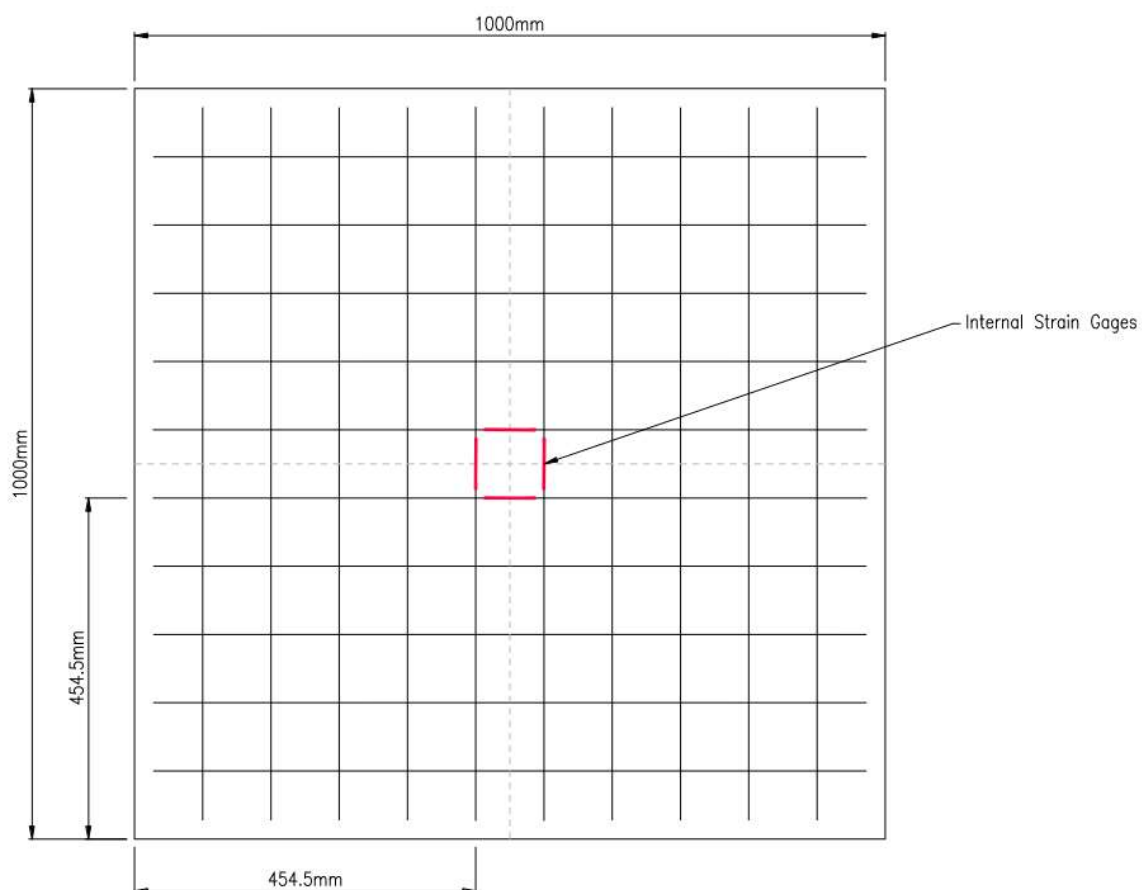


Figure 4.4: Internal Strain Gauge Locations

4.2.2 Force Sensors

Force sensors were employed to measure the impact force applied to the concrete slabs. These devices convert mechanical force into an electrical signal, allowing for accurate measurement and monitoring of forces in various applications.

For this experiment, two force sensors were utilised, however they were placed within a protective plate assembly as they were required to be reused with every test. The assembly consisted of a base plate where the force sensors were placed, then a protective plate which was screwed into place to ensure it was resting securely on top of the sensors. This required the development of two “fake” sensors to balance the plate and spread the impact force evenly (Figure 4.5).

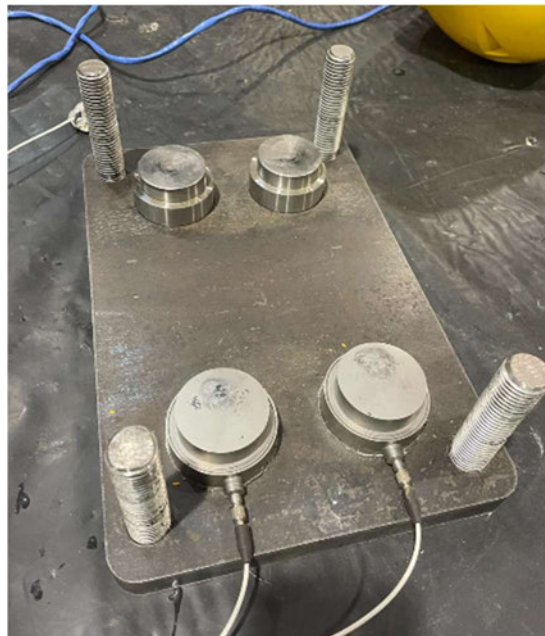


Figure 4.5: Force Sensors and Protection Assembly

4.3 Test Methodology

Using a crane, each specimen was positioned under the test frame with a crane where then sensors were attached, and the data recording equipment was set up. Completing the experiment setup was the loading of the 300kg drop hammer into the test frame using the crane. The completed test set up is depicted in Figure 4.2.

The execution of the impact test involved dropping the 300kg hammer from 2m high onto the midpoint of the first concrete slab (S1), data was recorded then the specimen was unloaded, the test frame was reset, and the procedure was repeated for the other two slabs (S2 and S3).

Chapter 5 Observations, Results and Discussion

5.1 Chapter Overview

This chapter will analytically evaluate the data collected from the experiment. Simple mathematical and dynamic force principles will be employed to assess the energy absorption characteristics of each test sample. The dataset received includes impact force measurements, deflection values, and strain data. Additionally, the failure modes and cracking patterns of each slab will also be investigated.

5.2 Impact Test Results

The main objective of this experiment is to investigate the structural behaviour of concrete slabs reinforced with different GFRP bar diameters when subjected to an impact load. Table 5.1 summarises the maximum impact force, mid-point deflection, strain and acceleration values recorded. As illustrated in Table 5.1, all acceleration values recorded were the same, thereby verifying the consistent dropping of the hammer onto the test samples.

Specimen	Bar Diameter (mm)	Force (kN)	Strain	Acceleration (g)
S1	8	117.9	6307	101.186
S2	10	100.9	4926	101.186
S3	13	79.5	2278	101.186

Table 5.1: Summarised Test Results

5.3 Impact Force

Figures 5.1 to 5.6 depict the impact force versus time for all three test samples. Evidently, there is minimal disparity in maximum force levels between S1 and S2, while S3 exhibits notably lower force values in comparison to the previous two specimens.

When evaluating results from Force Sensor 1, a reduction of 14% in maximum force magnitude is observed between the force data measured for S1 and S2. Results from Force Sensor 2 revealed a substantial 80% reduction in maximum force for S2 relative to S1. For S3, a reduction of 33% (Force Sensor 1) and 27% (Force Sensor 2) in maximum force magnitude is observed when compared to S1. In contrast to S2, results from S3 indicates a decrease in peak force magnitude by 21%, while Force Sensor 2 indicates a 71% increase in force magnitude.

The decrease in impact force between slabs with larger reinforcement bar diameters can be attributed to the wider surface area the larger diameter bars provide as they allow the applied load to be distributed more evenly throughout the slab. This reduces the localised stress concentration and thus the overall impact force experienced by the test specimen. Another reason for this reduction in impact force is that the bars with larger diameter generally have higher tensile and flexural strength. This increased strength enables the slab to withstand the applied impact force without causing severe damage, resulting in a reduced impact force.

The impact force behaviour of each slab exhibits a degree of similarity, particularly in the case of S1 and S2. However, it is apparent that the dissipation of the impact forces from the hammer rebounding on the sample occurs more quickly in the case of S3. This is demonstrated by the following force recordings after the initial impact, which displayed lower magnitudes and a quicker decay.

The effective dissipation of the impact forces for the samples reinforced with larger GFRP bar diameters can be accredited to the reinforcements ability to absorb more energy due to their greater-cross sectional area. The energy absorption assists in reducing the rate of deceleration and spreading the impact force across a larger section of the slab, thus mitigating the energy. This is supported by outcomes revealed from a study completed by Xiao et al. (2017), where it was demonstrated that an increase in bar diameters lead to a decrease in impact force and localised stress as the larger area allows for the forces to be distributed more effectively.

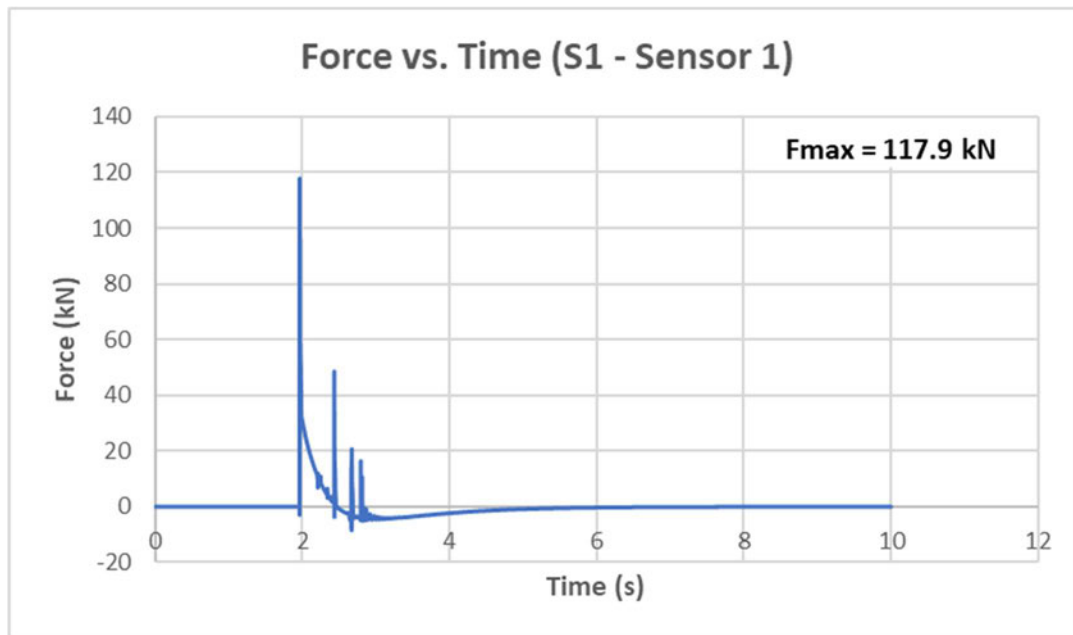


Figure 5.1: Force – Time Histories of S1 (Force Sensor 1)

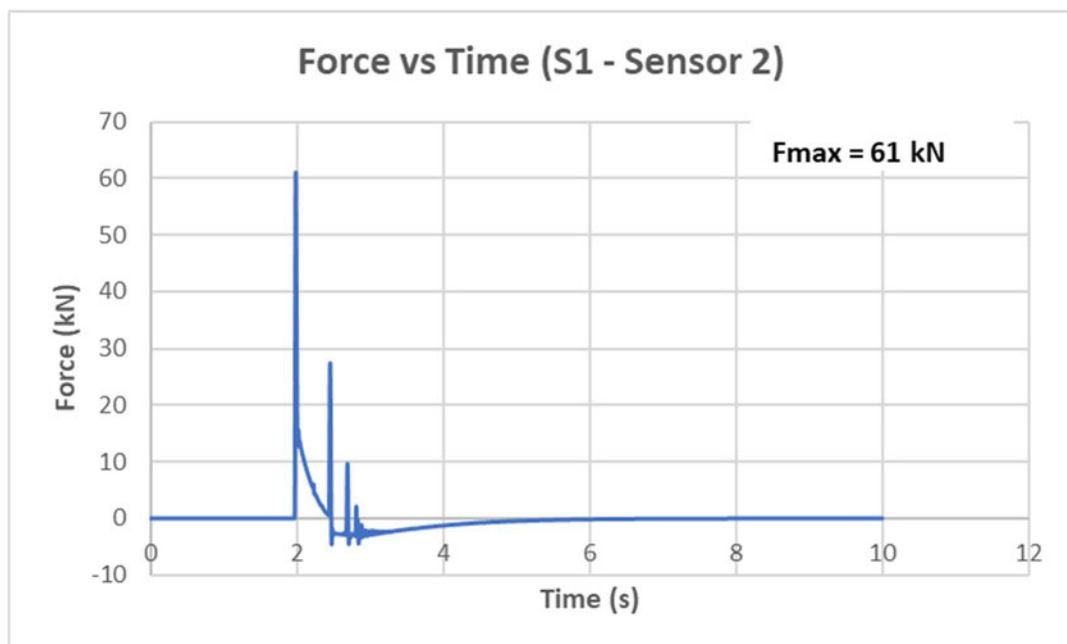


Figure 5.2: Force – Time Histories of S1 (Force Sensor 2)

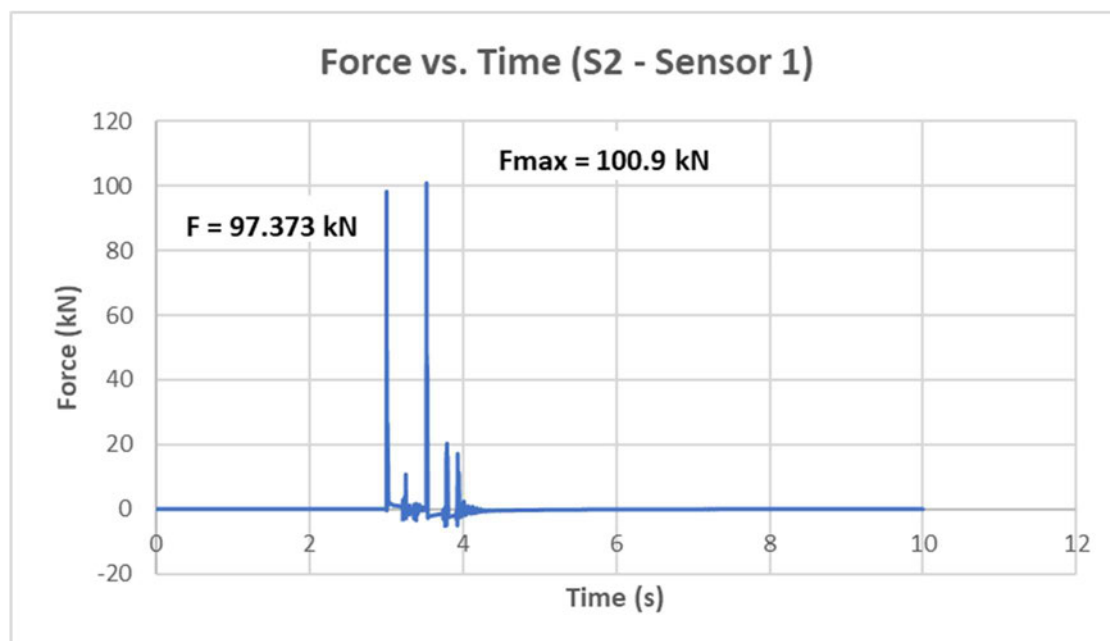


Figure 5.3: Force – Time Histories of S2 (Force Sensor 1)

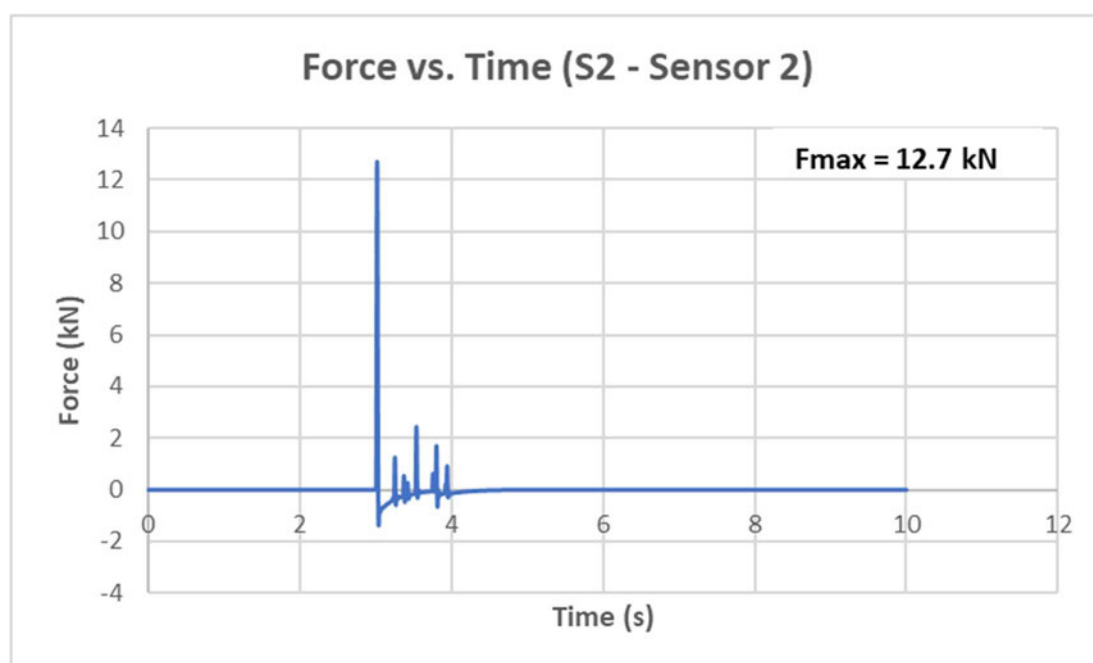


Figure 5.4: Force – Time Histories of S2 (Force Sensor 2)

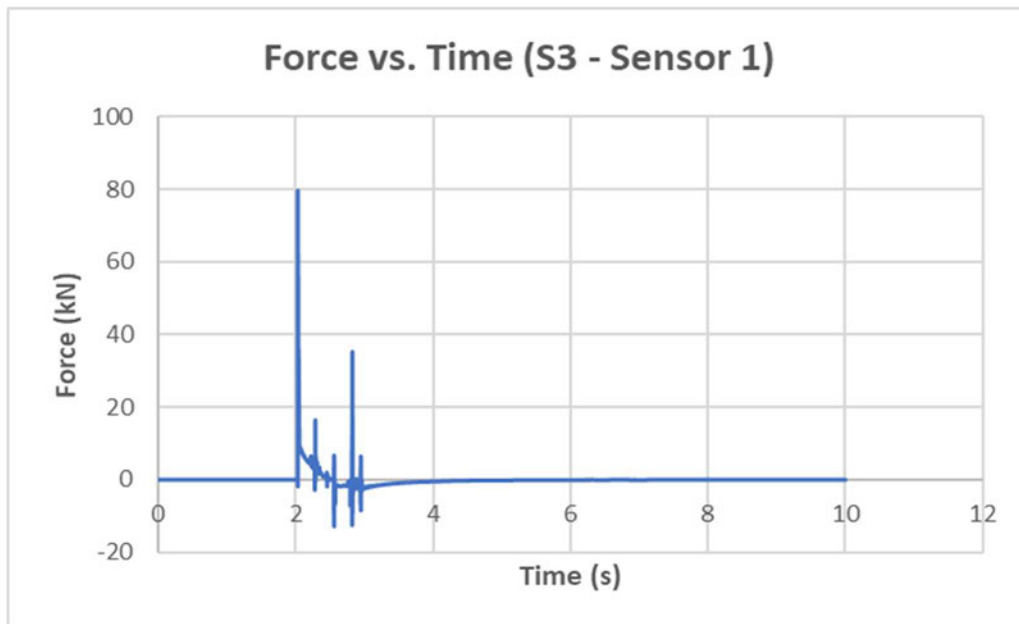


Figure 5.5: Force – Time Histories of S3 (Force Sensor 1)

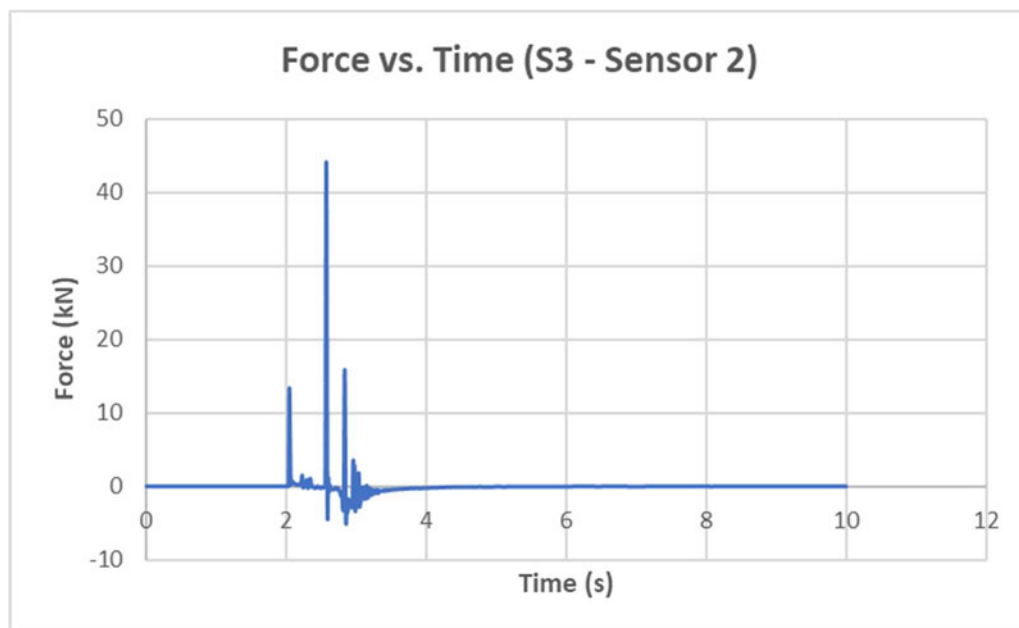


Figure 5.6: Force – Time Histories of S3 (Force Sensor 2)

5.4 Energy Absorption

Potential energy (PE) and kinetic energy (KE) are fundamental concepts in understanding the response of the concrete slabs when subjected to the drop weight impact load.

Potential energy refers to the energy the drop hammer possesses when it's lifted to a certain height above the concrete slab. The potential energy of the drop weight is calculated as follows;

$$PE = mgh$$

where;

m = drop weight mass (kg)

g = acceleration due to gravity (m/s^2)

h = drop height (m)

$$\Rightarrow PE = 300 \times 9.81 \times 2$$

$$PE = 5886 \text{ J}$$

Kinetic energy refers to the energy of an object in motion. When the object is released and accelerates due to gravity, the potential energy is converted into kinetic energy. The kinetic energy of the drop hammer is calculated as follows;

$$KE = \frac{1}{2}mv^2$$

where;

m = drop weight mass (kg)

v = impact velocity (m/s)

$$\Rightarrow v = \sqrt{2gh}$$

$$v = \sqrt{(2 \times 9.81 \times 2)}$$

$$v = 6.2642 \text{ m/s}$$

$$\Rightarrow KE = \frac{1}{2} \times 300 \times 6.2642^2$$

$$KE = 5886 \text{ J}$$

To assess the energy absorbed into the slabs, the impact force data was cleaned and simplified to only include data from the first initial impact drop until the first rebounding motion of the hammer. The energy absorbed by the test samples from the impact of the drop-weight is calculated by integrating the area under the force-time curve for each specimen.

S1 recorded its maximum impact force of 117.9kN at $t = 1.963$ s. When evaluating the force data, the force sensors recorded a value of zero at approximately 2.464s which is when the hammer was about to rebound. This simplified impact force behaviour is represented in Figure 5.7.

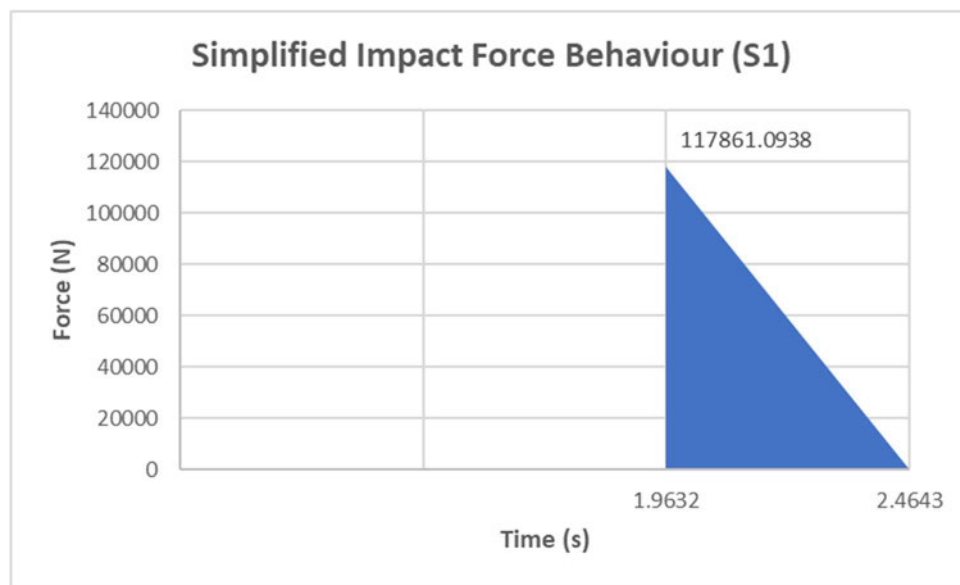


Figure 5.7: Impact – Force Curve (S1)

The following calculations were completed to calculate the energy absorbed by S1;

$$\begin{aligned}
 \text{Energy} &= \int_b^a (F \times dt) \\
 \text{Energy} &= \int_{1.9632}^{2.4643} (F \times dt) \\
 &= \frac{1}{2} \times 117861.09 \times (2.4643 - 1.9632) \\
 \text{Energy} &= 29,530.09 \text{ J}
 \end{aligned}$$

S2 recorded its maximum impact force of 100.9kN at $t = 3.524$ s, however this value was from the rebound impact. According to force sensor 1 for S2, the impact force magnitude the slab experienced was 97.373kN at $t = 3$ s. When evaluating the force data, the force sensors recorded a value of zero at approximately 3.241s which is when the hammer was about to rebound. This simplified impact force behaviour is represented in Figure 5.8.

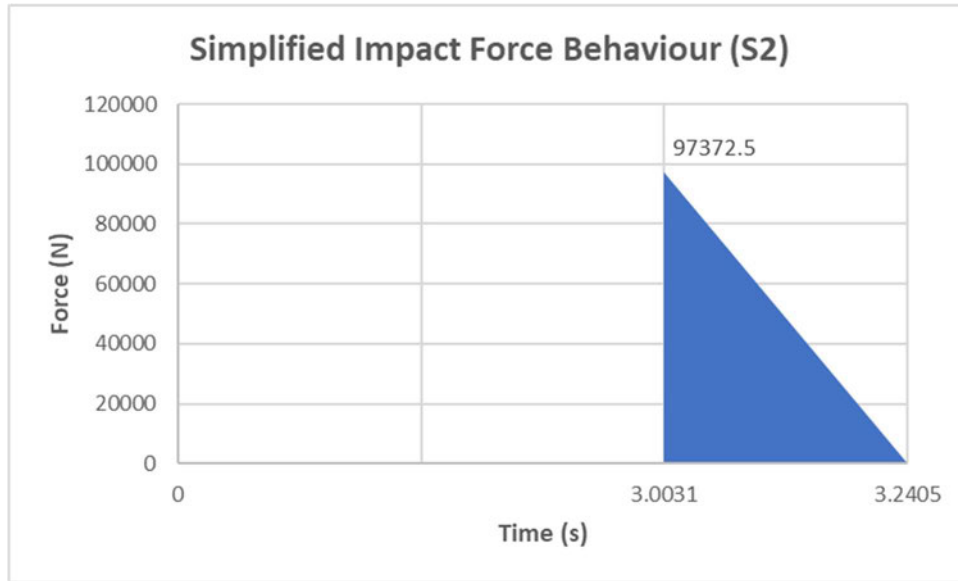


Figure 5.8: Impact – Force Curve (S2)

The following calculations were completed to calculate the energy absorbed by S2;

$$\begin{aligned}
 \text{Energy} &= \int_b^a (F \times dt) \\
 \text{Energy} &= \int_{3.0031}^{3.2405} (F \times dt) \\
 &= \frac{1}{2} \times 97372.5 \times (3.2405 - 3.0031) \\
 \text{Energy} &= 11,558.12 \text{ J}
 \end{aligned}$$

S3 recorded its maximum impact force of 79.5kN at t = 2.031s. When evaluating the force data, the force sensors recorded a value of zero at approximately 2.53s, indicating the hammers rebounding action. This simplified impact force behaviour is represented in Figure 5.9.

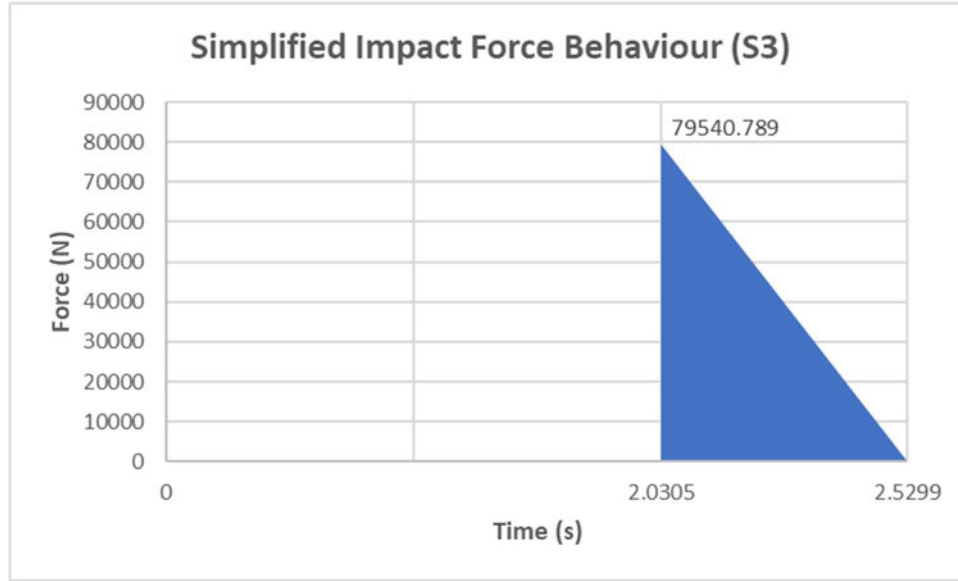


Figure 5.9: Impact – Force Curve (S3)

The following calculations were completed to calculate the energy absorbed by S3;

$$\begin{aligned}
 \text{Energy} &= \int_b^a (F \times dt) \\
 \text{Energy} &= \int_{2.0305}^{2.5299} (F \times dt) \\
 &= \frac{1}{2} \times 79540.789 \times (2.5299 - 2.0305) \\
 \text{Energy} &= 19,861.34 \text{ J}
 \end{aligned}$$

When evaluating the energy absorbed by each test specimen in relation to the calculated kinetic energy, all samples absorbed a considerable amount more of energy than the calculated 5,886 J of kinetic energy. S1 absorbed 29,530 J which is 80% more than the determined KE value, Slab 2 absorbed 11,558 J which is 50% more than the calculated KE and lastly, Slab 3 absorbed 19,861 J which is 70% more than the determined KE.

Based on these results, it would indicate the S1 experienced the most amount of deformation or damage, then S3 with S2 absorbing the least amount of energy. Factors that would explain why a slab reinforced with larger bars would result in rebounding is if they are unable to deform significantly and are more rigid in nature. This behaviour is supported by research conducted by Sadraie et al. (2019) who demonstrated that increasing the reinforcement ratio provided more stiffness and rigidity. Slab 3 consists of larger diameter reinforcement and is able to distribute the load more evenly throughout the slab. This response is supported by research conducted by

This uniform distribution results in a potentially higher level of resistance to deformation which can contribute to the hammer rebounding. Conversely, S1 is likely to absorb more energy and may be less likely to cause rebounding as the slab is more ductile and the internal reinforcement can deform more efficiently to absorb the energy.

Upon impact, the kinetic energy from the drop-weight is transferred to the concrete slab. The concrete slab absorbs the energy, leading to deformation and cracking, and then the excess energy is reflected, resulting in the hammer rebounding. The results from the impact force data and the calculated absorbed energy verifies that the energy capacity of all three specimens was exceeded and led to the hammer to rebound until coming to a rest atop the slab.

It is important to note that there is an incongruity in the accuracy of determining the energy absorption based on the slabs impact force data. Theoretically, the impact force of the drop hammer is calculated as follows:

$$\text{Impact Force} = \frac{\text{Kinetic Energy}}{\text{Distance}}$$

$$F = \frac{5886}{2} = 2943 \text{ N}$$

This is verified by using Newton's Second Law of Motion;

$$F = ma$$

$$F = 300 \times 9.81 = 2943 \text{ N} \quad [OK]$$

All three test samples recorded impact force values that exceeded the theoretical prediction, which had anticipated the slabs to experience 2,943N of force from a 300kg hammer that is dropped from 2m high.

There are two potential explanations for this discrepancy including real-world variability and dynamic effects. When completing theoretical calculations, it is assumed that the experiment is to be conducted in idealised conditions. However, real world situations are vulnerable to uncertainty and variability. Factors such as surface conditions, equipment limitations and human error are likely causes for inaccuracies or contrasts between theoretical expectations and actual measurements. Dynamic effects refer to how dynamic forces are not always accurately reflected by theoretical models. This is due to the abrupt and dynamic nature of impact loads which can result in force spikes or transient reactions that may exceed theoretical predictions.

5.4 Deflection

Figure 5.10 to 5.13 shows the deflection versus time results for all three slabs. The midpoint deflection profiles provide a good indicative measure to show the influence of the reinforcement ratio within each respective slab. The midpoint also corresponds to the impact location, as the hammer was dropped at the central point of each specimen.

Table 5.2 summarises the deformation behaviour exhibited by the test samples across three different phases. The initial phase is the deflection recorded at the moment of initial impact. The second phase corresponds to the deflection observed during the hammer's rebound when the slab behaves elastically and attempts to regain its original form. Finally, the third phase is the maximum deflection recorded. This refers to the specimen's response when the hammer remains in place atop the slab following the completion of the drop.

Specimen	Phase 1		Phase 2		Phase 3	
	Deflection (mm)	Time (s)	Deflection (mm)	Time (s)	Deflection (mm)	Time (s)
S1	21.07	2.94	20.70	3.04	33.19	3.58
S2	9.87	3.82	6.92	4.08	12.39	4.52
S3	1.58	3.26	0.72	3.5	12.20	3.88

Table 5.2: 3-Phase Deflection Results

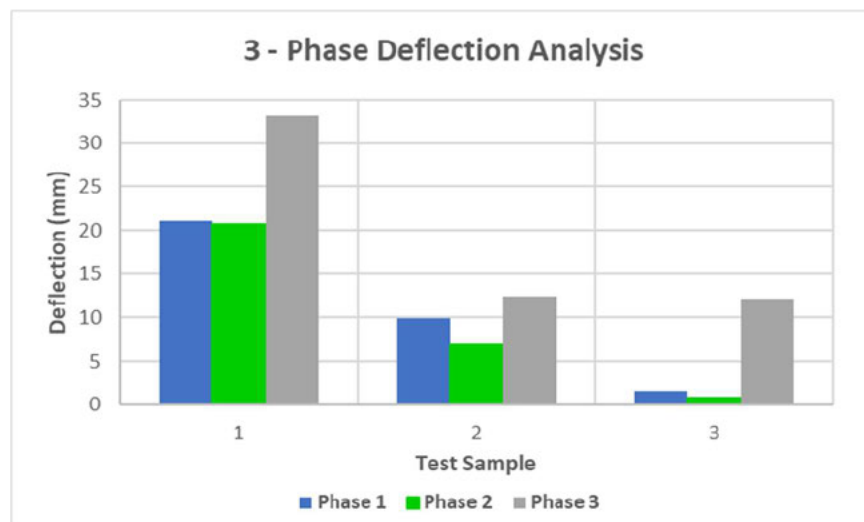


Figure 5.10: 3-Phase Deformation History

In terms of the slab's response during the initial impact, S1 recorded a deflection value of 21.07mm, S2 recorded a deflection value of 9.87mm which is 54% less than S1. Notably, S3 recorded the lowest maximum deflection value of 1.58mm which is 93% less than that of S1 and 84% less than that of S2. These results indicate that slabs reinforced with larger diameter bars are stiffer in nature thereby decreasing the specimen's deflection when subjected to an impact load. Conversely, S1 which is reinforced with small diameter bars, resulted in localised stress concentrations which leads to more significant deflection. This outcome is confirmed with the findings presented by Sadraie et al. (2019) which demonstrated that an increase in the reinforcement ratio results in a decrease in maximum deflection.

As the hammer rebounded after the initial impact and the slab began to return to its original form, the deflection values progressively decreased. S1 recorded a deflection of 20.70mm which is 2% less than its deflection when the impact occurred. S2 exhibited a deflection value of 6.92mm in the second phase, which is a reduction of approximately 30% in deflection. Lastly, S3 presented a deflection reading of 0.72mm in this phase, marking a sizable reduction of 55% compared to the deflection recorded during impact phase. Both S2 and S3 demonstrated elastic behaviour in response to the hammer rebounding. In contrast, S1's deflection did not substantially decrease indicating that the smaller bars induce a more inelastic behaviour under the impact load. This resulted in a higher deflection value as the reinforcement underwent plastic deformation.

S1 in the final phase presented a residual deflection value of 33.19mm, signifying an increase of 37% in contrast to the deflection recorded during the impact and 38% compared to the deflection value obtained as the hammer rebounded. S2 presented a residual deflection value of 12.39mm which is 21% higher than the deflection recorded during impact and 45% higher than the deflection recorded as the hammer rebounded. Notably, this deflection reading was also 63% less than the residual deflection recorded for S1. Lastly, S3 revealed a residual deflection value of 12.2mm. This value is 87% higher than the deflection recorded during the impact and is also 94% higher than the deflection value recorded as the hammer rebounded. In contrast to the residual values obtained from S1, S3 recorded a reduction of deflection by 64%. However, S3 and S2 presented very similar residual results with S3 displaying a deflection value only 2% less than that of S2.

The residual deflection results for all three test samples indicate that S1 underwent plastic deformation during the impact. This is clear as the maximum residual deflection recording for all three samples was S1, which included the deflection from the initial impact when the bars plastically deformed plus the deflection from the hammer resting on top of the slab. This is reflected by the fact that S2 and S3 recorded different deflection values during the initial impact and rebound phases but resulted in similar residual deflection values. This suggests that neither S2 or S3 incurred plastic deformation and that the residual deflection is just a measurement of the hammer causing deflection while resting on the slab.

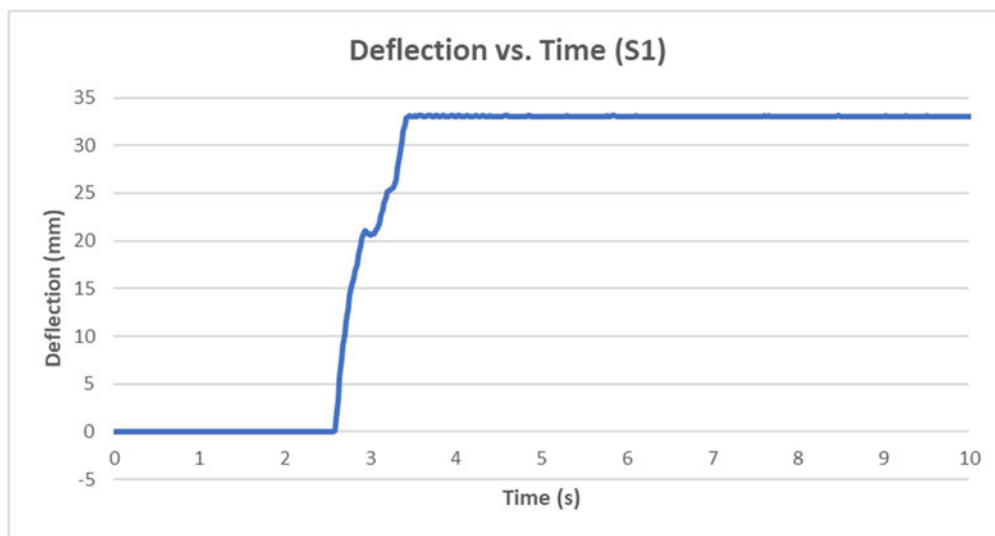


Figure 5.11: Deflection – Time History of S1 (8mm)

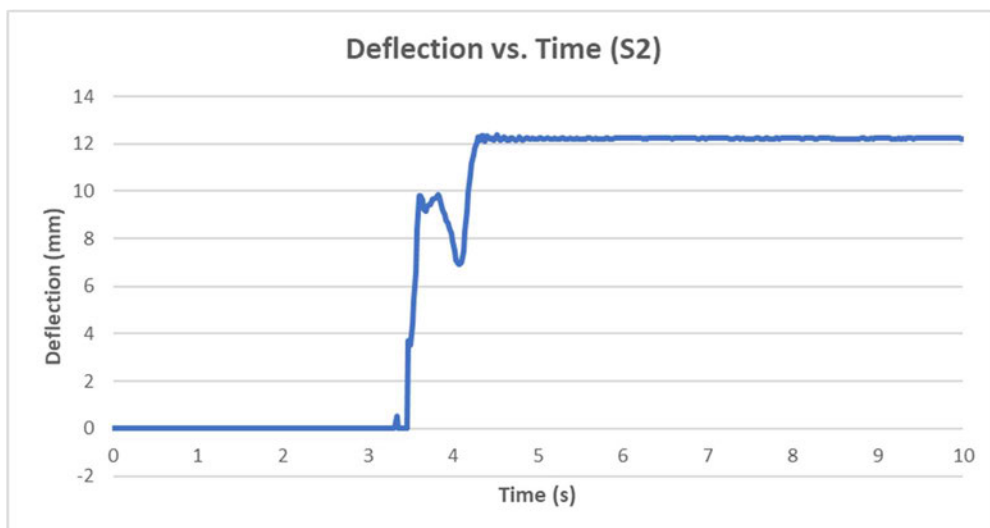


Figure 5.12: Deflection – Time History of S2 (10mm)

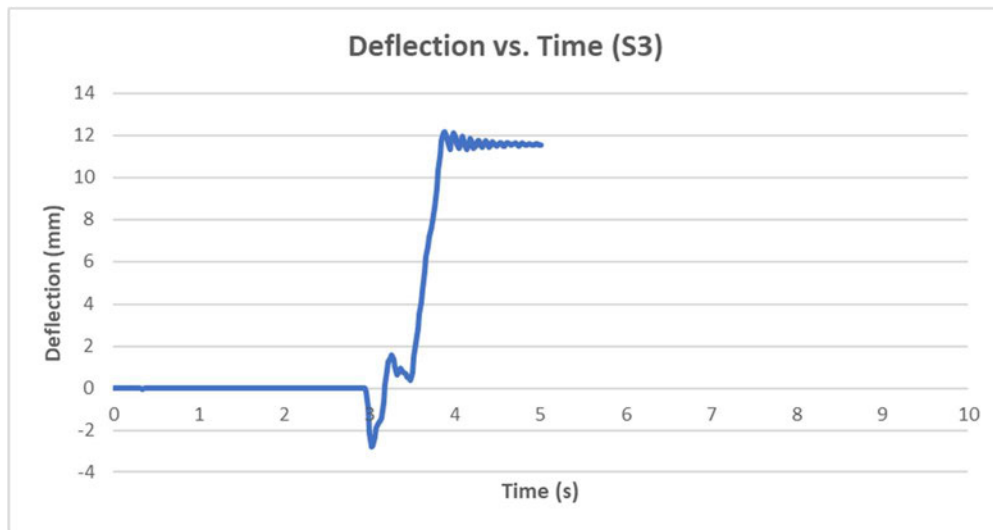


Figure 5.13: Deflection – Time History of S3 (13mm)

5.5 Strain Data

Figures 5.14 to 5.16 displays the strain data in regard to time from the experiment. To monitor the strain distribution and variations, each test sample consisted of four internal strain gauges and two external strain gauges. However, there is a portion of data absent in some samples due to the damage incurred by the measurement devices during the impact test.

There are notable similarities in response patterns when evaluating the strain data obtained for all three specimens. The external strain gauges generally recorded low values of strain. Conversely, the internal strain gauges attached to the internal reinforcement recorded the most significant strain values from each specimen. The evaluation of the strain data is broken into two parts for each specimen. The first segment involving the maximum strain encountered during the initial impact and then the residual strain value when the hammer had ceased rebounding and is resting on the slab.

In the case of S1, the maximum strain was recorded by internal device 3, yielding a reading of 6307, with a residual recording of 2351. In contrast, data from S2 unveiled a maximum strain reading of 4926, which was also recorded by internal device 3. The residual strain value for S2 was 3150. This magnitude represents a reduction in strain of approximately 22% and an increase in strain of 26% when compared to S1. Similarly, S3 results presented a maximum strain measurement of 2278 and a residual strain value of 1585, originating from internal device 2. The maximum strain value displays a reduction of approximately 64% compared to the

maximum strain recorded in S1 and a 54% reduction relative to the maximum strain observed in S2. In terms of residual strain, S3's results are 33% less than S1 and 50% less than S2.

The test samples reinforced with larger diameter bars exhibited less strain during the impact test due to a variety of factors. Firstly, the larger bars are more efficient in reducing localised stress concentrations than smaller diameter bars. This is why S1 recorded higher levels of strain in the centre of the slab as the smaller bars were not effective in dispersing the impact. S3 experienced lower amounts of strain as the larger diameter bars have a higher load carrying capacity and therefore the slab doesn't need to deform as much to accommodate the applied force. However, a notable response was the residual strain recording from S2 which was higher in contrast to data from S1. This result may potentially be accredited to the smaller bar diameters exhibiting higher levels of ductileness and greater potential for elastic deformation. This suggests that the smaller diameter bars absorb the impact force with less residual strain as they are more capable to return to their original state after the impact load is complete.

The values of the external strain gauges are negative as the strain gauges work in a differential mode with one type of gauge experiencing tension while the other type experiences compression. In this experiment the external gauges attached to the top face of the samples were set to compression mode. When evaluating the strain data recorded from the external gauges, S1 recorded a maximum value of -1211 and a residual value of -698, S2 resulted in a maximum value of -450 and a residual value of -326 and lastly S3 recorded a maximum strain value of -845 and a residual value of -739.

As for the results recorded from the gauges attached on the compressive side of the specimens, the high values of strain recorded from S3 indicate that the larger diameter bars are generally more rigid in nature. When the impact load was applied, S3 resisted straining internally, allowing for an increase of strain on the compressive side of the slab. This response may also be an indication of poor bonding between the bars with larger diameters and the concrete as this reduces the efficiency of the impact load transferring and can theoretically lead to increased strain levels. This is supported by research conducted by Gu, Yu and Wu (2016) which determined that increasing the bar diameter reduced the peak bond strength.

The strain data obtained from S2 was less than the strain values recorded for S1. This response may be due to the increased potential for elastic deformation that smaller diameter bars hold. This flexible behaviour enables the slab to absorb the impact by deforming more internally and reducing the strain externally. The findings from this investigation are supported by research conducted by Said and Mouwainea (2022) and Khorramaian and Sadeghian (2017) whose study revealed that the GFRP bars only reached 50% of their predicted strain capacity.

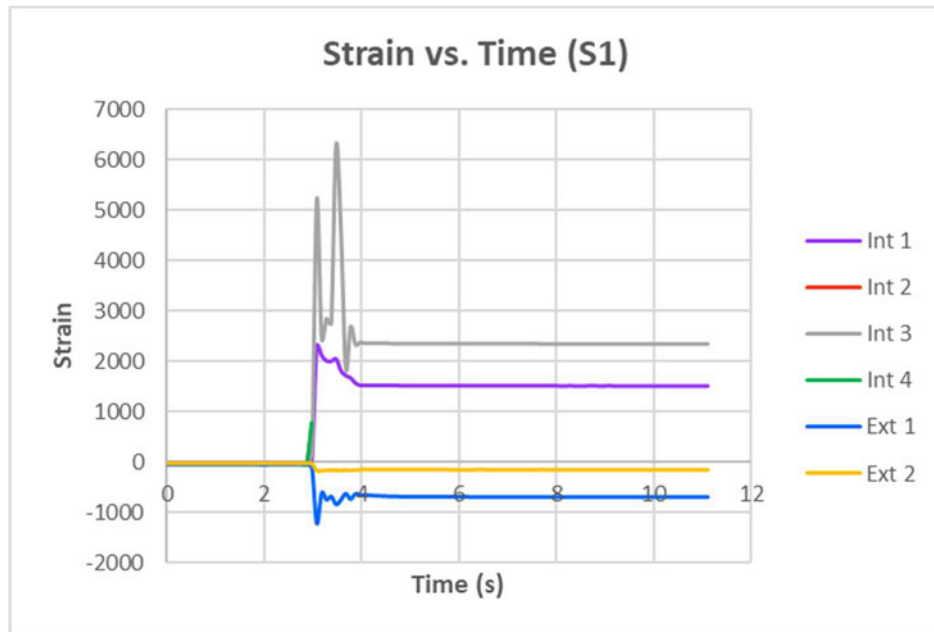


Figure 5.14: Strain – Time History of S1 (8mm)

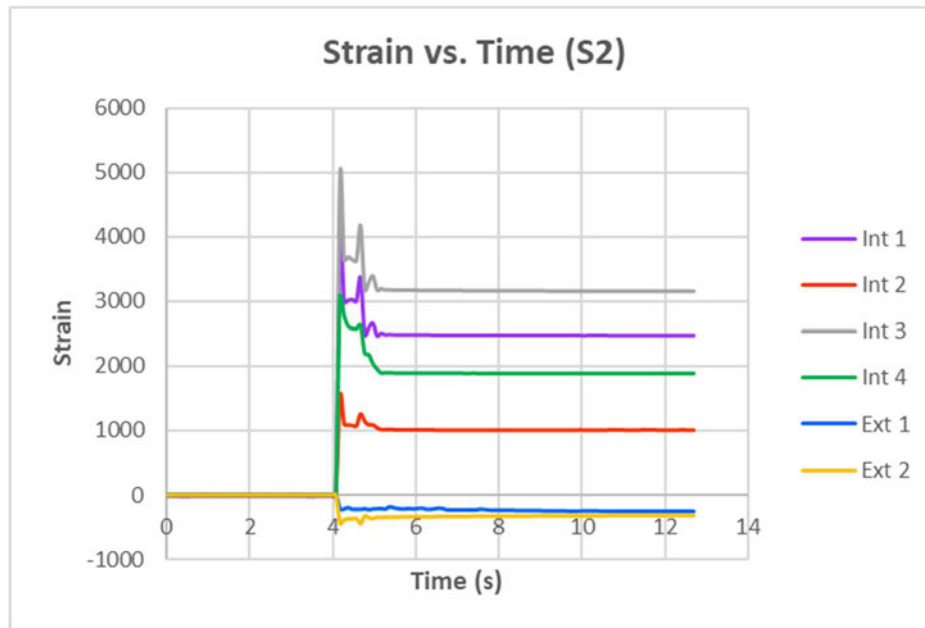


Figure 5.15: Strain – Time History of S2 (10mm)

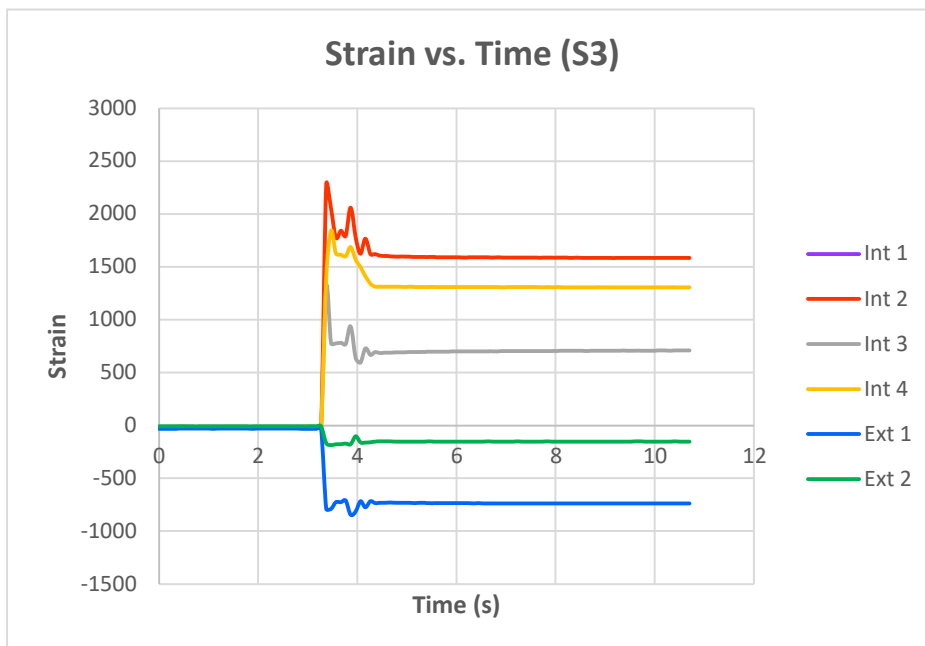


Figure 5.16: Strain – Time History of S3 (13mm)

5.7 Cracking Pattern and Failure Mode

S1 presented a combination of cracking in the tensile zone and shear failure. In contrast to the other two test samples, the cracking pattern of S1 was primarily localised towards the central impact zone as depicted in Figure 5.17. This indicates that the smaller diameter bars reinforcing the slab were less efficient in uniformly transferring the energy and force throughout the slab. Minor scabbing was observed on the underside of Slab 1, indicating punching shear. Furthermore, the cracks on the underside were observed to be slightly wider compared to the damage the other specimens displayed.

S2 revealed less intense cracking with a more even distribution of cracking across the samples side face. The damage resembled S1, with a concentration of tensile cracking and signs of shear failure. Interestingly, this was the only sample to exhibit minor scabbing on both the side and underside of the slab.

S3 yielded the best results, demonstrating minimal damage from the impact force. There was a reduction in both tensile cracking and shear failure in contrast to the two previous slabs tested. The cracks on the underside of the slab were also the least severe however the pattern was similar to both S1 and S2 (Figure 5.19)

In comparison to the preliminary test results, none of the test samples presented visible signs of the reinforcement yielding. As expected, none of the samples perforated and no spalling occurred on the compression sides of the slabs.

The effect of increasing the reinforcement bar diameters under these loading conditions revealed that the slab reinforced with the largest diameter was the most resistant to local damage. The cracking pattern of S3 was less severe to the previous two slabs, implying that the larger diameter bars are more effective in minimising stress concentration areas and decreasing propensity of cracks. The observations were similar to those from research conducted by Said and Mouwainea (2022) and Delhomme et al. (2005). It is also supported by research conducted by Salih et al. (2022) which revealed that lower strain recordings in GFRP reinforced slabs (such as S3 strain results) resulted in improved crack control and enhanced durability.

Conclusively, the response of are suggests that the increased strength provided from the larger diameter bars within the slab is directly related to its ability to withstand and counteract higher impact loads before experiencing cracking and other forms of structural damage. This is supported by a study completed by Gribniak, Rimkus, Torres and Hui (2018) which revealed that a decrease in stiffness provided by smaller diameter GFRP bars results in an increase of slab deformation and greater cracking. This is an unfavourable outcome as cracking is the primary cause of deterioration in reinforced concrete structures as it allows moisture to invade the concrete (Gribniak, Rimkus, Torres and Hui 2018).

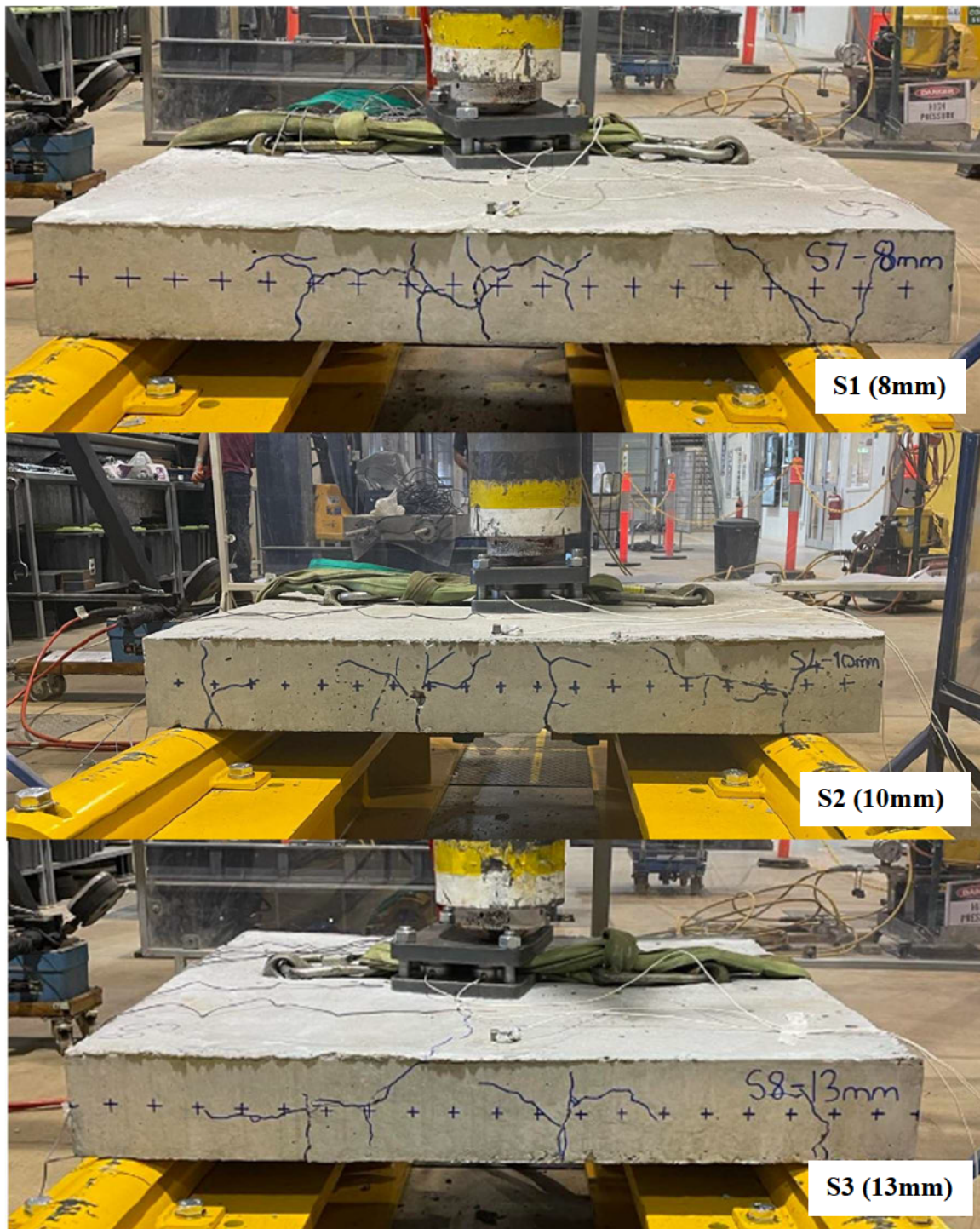


Figure 5.17: Cracking Pattern of Test Slabs (Side Face)

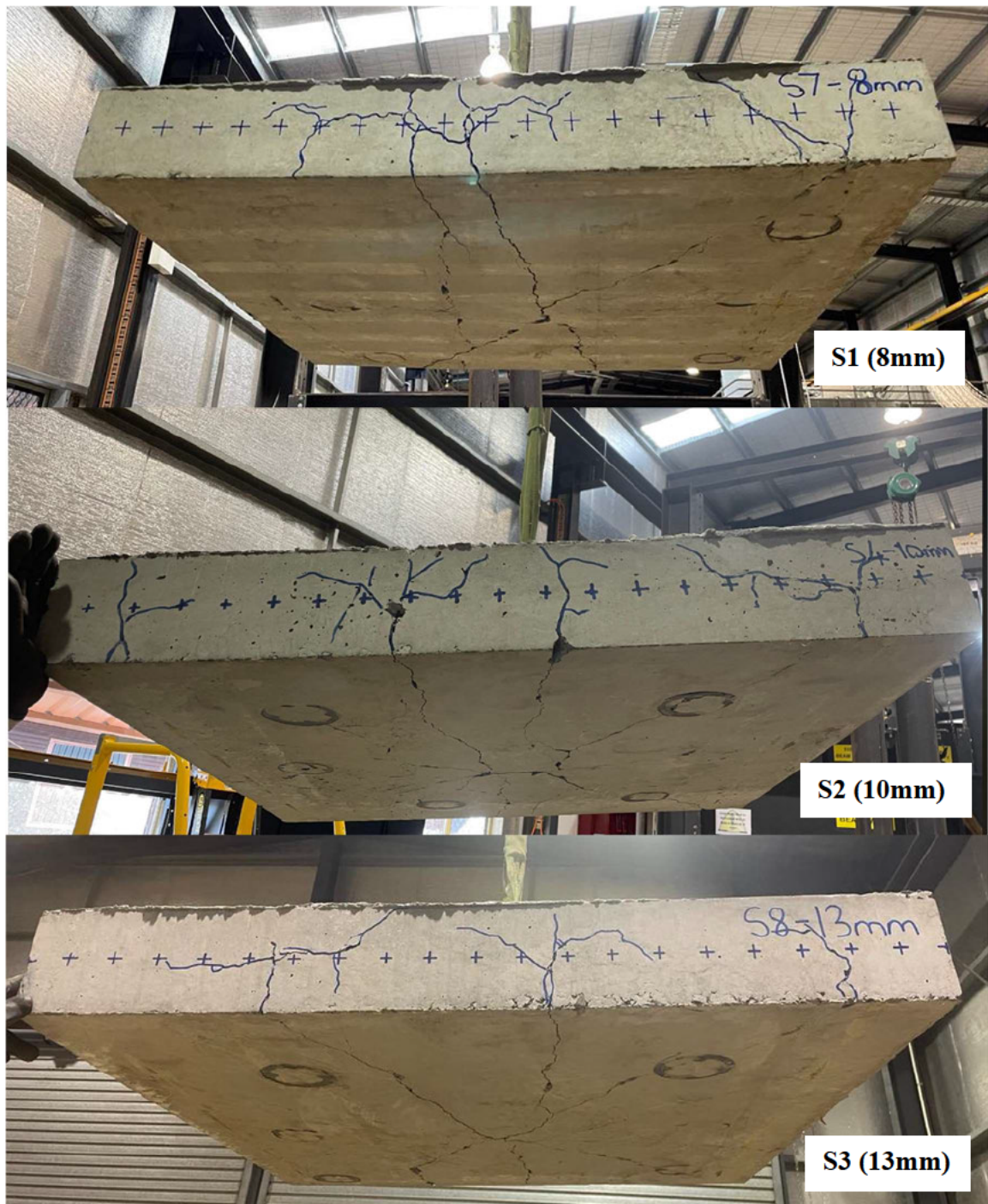


Figure 5.18: Cracking Pattern of Test Slabs (Angled View)

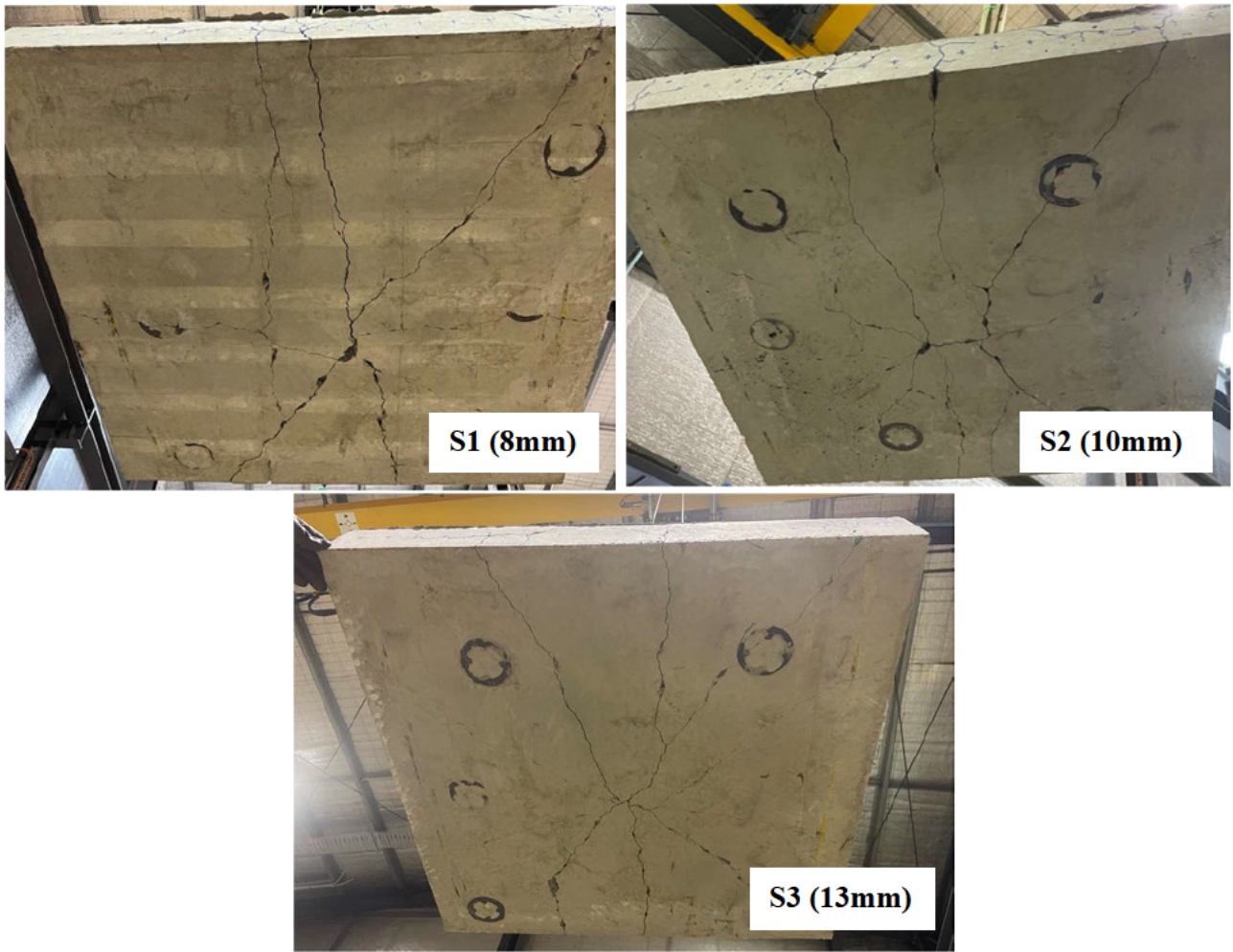


Figure 5.19: Cracking Pattern of Test Slabs (Bottom Face)

Chapter 6 Conclusion

5.1 Key Project Outcomes

This study comparatively evaluated the structural performance of concrete seawalls reinforced with different GFRP bars when subjected to impact loading conditions. It focused on evaluating the impact force, energy capacity, deflection, strain, and failure behaviour of the test samples. The following conclusions can be drawn from this study:

- A reduction in impact force is attributed to an increase in GFRP bar diameter. S3 presented maximum impact force values 33% and 21% less in comparison to S1 and S2.
- Specimens reinforced with larger bar diameters are more effective in dissipating the initial impact force by dispersing the impact energy across a larger section of the slab and thereby reducing the rate of deceleration of the hammer rebounding.
- Impact force data and simplified energy calculations validate that the energy capacity of all three test samples were exceeded, resulting in the hammer to rebound until coming to rest atop the slabs.
- More energy was absorbed into slabs reinforced with smaller diameter bars as they are more ductile in nature and can deform more effectively to absorb the energy.
- S3 was more resistant to deflection during the impact tests. This is potentially due to the increase in slab stiffness and indicates that the larger diameter bars are more efficient in dispersing the impact load.
- In response to the hammer rebounding, S1's deflection did not decrease considerably from the deflection recorded during the initial impact, indicating inelastic behaviour and plastic deformation. Furthermore, S2 and S3 recorded similar residual deflection data, signifying that no plastic deformation occurred and that the residual deflection for these two samples was caused by the hammer resting atop the slab. Conversely, S1 recorded the maximum residual deflection, indicating the slab underwent plastic deformation during the impact.
- Specimens reinforced with larger bar diameters were more effective in reducing local stress concentrations with S3 recording maximum strain values 64% and 54% less than values presented from S1 and S2.

- An increase in strain recorded from the external gauges indicates that the increase of stiffness and rigidity provided from the larger diameter bars lead to an increase in strain on the compression sides of the samples. This can potentially be accredited to the poor bonding between larger GFRP reinforcement bars and the concrete.
- The smaller diameter GFRP bars used were less successful in uniformly transferring the force throughout the slab. S1 demonstrated a combination of cracking in the tensile zone and shear failure, with a concentration of localised cracking in the central impact zone.
- Visual observations of S3's response to the impact load verifies that the increase of bar diameter does result in an increase in ability to withstand and counteract higher impact loads before cracking. Additionally, the cracking pattern of S3 was less severe than previous specimens tested, suggesting that the increase in bar diameter leads to a reduction in stress concentration areas and minimises the propensity of cracks.

5.2 Future Work

Although there is a considerable amount of research relating to the flexural, shear and torsional behaviour of GFRP bars, there still remains a noticeable gap in the understanding of GFRP-reinforced concrete's response to dynamic loading conditions. Impact resistance is an important aspect of structural performance, specifically in regard to research relating the performance of seawalls when subjected to intense wave action forces and vessel collisions during extreme weather events.

The number of studies dedicated to investigating the impact behaviour of GFRP-reinforced concrete is limited. This deficiency is research stresses the need for further exploration and evaluation of GFRP-reinforced concrete under dynamic and impact loading conditions to comprehensively assess its suitability for diverse structural applications.

Further research that can be conducted to improve the design of seawalls includes investigating the following parameters;

- Altering the reinforcement quantity and configuration
- Varying concrete strengths of slabs reinforced with GFRP bars.
- Dynamic response of other Fibre Reinforced Polymer (FRP) bars
- Comparing the behaviour of GFRP bars to other FRP materials and to the structural performance of traditional steel reinforcement.
- Adjusting the drop height and hammer mass.
- Repeated impact loading conditions

Focusing on this knowledge gap concerning the impact behaviour of GFRP reinforced concrete will further develop the pertinency of this innovative material, paving the way for safer and more durable infrastructure in the future.

References

Abed, F, Mehaini, Z, Oucif, C, Abdul-Latif, A & Baleh, R 2020, '*Quasi-static and dynamic response of GFRP and BFRP bars under compression*', Composites Part C: Open Access, vol.2, viewed 4 May 2023, <
<https://www.sciencedirect.com/science/article/pii/S2666682020300347#:~:text=GFRP%20bars%20exhibited%20compressive%20strength,BFRP%20bars%20was%20470%20MPa>>.

Alachek, I, Reboul, N & Jurkieweiz 2018, '*Bond strength's degradation of GFRP-concrete elements under aggressive exposure conditions*', Construction and Building Materials, vol.179, pp.512-525, accessed 6 September 2023, <
<https://www.sciencedirect.com/science/article/pii/S0950061818313357>>.

Australian Bureau of Statistics 2018, *Population Projections*, Australia, ABS, viewed 27 March 2023, < <https://www.abs.gov.au/statistics/people/population/population-projections-australia/latest-release#cite-window1>>.

Bangash, M 1993, '*Shock, impact and explosion: structural analysis and design*', Berlin: Springer, viewed 2 August 2023.

Bank, L 2006, '*Composite for construction: structural design with FRP materials*', John Wiley & Sons, viewed 17 Jul. 23, <
https://books.google.com.au/books?hl=en&lr=&id=1B2mTpDtUoAC&oi=fnd&pg=PR13&ots=7mNGwQueJG&sig=ZRB7AqP5Hok7ZHSstYpEqWDIm8&redir_esc=y#v=onepage&q&f=false>.

Benmokrane, B, Manalo, A, Bouhet, J, Mohamed, K & Robert, M 2017, '*Effects of Diameter on the Durability of Glass Fiber-Reinforced Polymer Bars Conditioned in Alkaline Solution*', Journal of Composites for Construction, vol.21, no.5, viewed 17 July 2023 <
<https://ascelibrary-org.ezproxy.usq.edu.au/doi/full/10.1061/%28ASCE%29CC.1943-5614.0000814>>.

Carmody, J & De Poloni, G 2018, '*WA storm cuts power, hits homes and washes yachts ashore as cold front strikes near Perth*', ABC News, 5 June, viewed 29 April 2023, <
<https://www.abc.net.au/news/2018-06-05/power-out-homes-damaged-as-big-cold-front-threatens-wa/9834952>>.

Chapman, M & Underwood, A 2011, *'Evaluation of ecological engineering of "armoured" shorelines to improve their value as habitat'*, Journal of Experimental Marine Biology and Ecology, vol.400, no.2, pp.302-313, viewed 1 May 2023, <
https://www.sciencedirect.com/science/article/pii/S0022098111000736?casa_token=olapIcrdRcAAAAA:Ds0XBzAh4RoKHOWp3jFcO0MBxbN4MdCdWmZflmfQEWG1UBoVRVsJsQnfH-LHAaOR0U7lKb_42XU>.

Couzens, G 2017, *'Huge oil spill after car ferry carrying 140 passengers' smashes into harbour wall in Gran Canaria after engine failure'*, The Sun, United Kingdom, 22 April, viewed 29 April 2023, <
<https://www.thesun.co.uk/news/3387936/huge-oil-spill-car-ferry-140-passengers-smashes-harbour-wall-gran-canaria/>>.

Fergani, H, Di Benedetti, M, Mias, C, Lynsdale, C & Guadagnini, M 2018, *'Durability and degradation mechanisms of GFRP reinforcement subjected to severe environments and sustained stress'*, Construction and Building Materials, vol. 170, pp. 637-648, accessed 6 September 2023, <
https://www.researchgate.net/publication/324130080_Durability_and_degradation_mechanisms_of_GFRP_reinforcement_subjected_to_severe_environments_and_sustained_stress>.

Gainsford, J, 2015, *'Repairs to Cronulla sea wall defects could cost \$1 million'*, The St George & Sutherland Shire Leader, 3 September, viewed 1 May 2023, <
<https://www.theleader.com.au/story/3323125/repairs-to-cronulla-sea-wall-defects-could-cost-1-million/>>.

Geoscience Australia 2011, *Australia's Coastline: adapting to climate change*, AusGeo News no.101, Australian Government, Canberra, viewed 27 March 2023, <
<https://www.ga.gov.au/ausgeonews/ausgeonews201103/climate.jsp#:~:text=More%20than%2080%20per%20cent%20of%20Australians%20live%20within%20the%20coastal%20zone>>.

Goldston, M, Remennikov, M & Neaz, S 2016, *'Experimental investigation of the behaviour of concrete beams reinforced with GFRP bars under static and impact loading'*, Engineering Structures, vol.113, pp.220-232, viewed 4 August 2023, <
<https://www.sciencedirect.com/science/article/pii/S0141029616000602>>.

Gribniak, V, Rimkus, A, Torres, L & Hui, D 2018, *'An experimental study on cracking and deformations of tensile concrete elements reinforced with multiple GFRP bars'*, vol.201, pp.477-485, accessed 6 September 2023, <
<https://www.sciencedirect.com/science/article/pii/S026382231831256X>>.

Gu, X, Yu, B & Wu, B 2016, '*Experimental study of the bond performance and mechanical response of GFRP reinforced concrete*', Construction and Building Materials, vol.114, pp.407-415, accessed 6 September 2023, <<https://www.sciencedirect.com/science/article/pii/S0950061816305153>>.

Hair, J 2017, *Cyclone Debbie photos capture trail of destruction across north Queensland*, digital images, ABC News, viewed 29 April 2023, <<https://www.abc.net.au/news/2017-03-29/cyclone-debbie-aftermath-gallery/8395494>>.

Hollaway, L 2008, '*Advanced fibre polymer composite structural systems used in bridge engineering*', ICE Manual of Bridge Engineering, pp. 503-529, viewed 17 July 2023, <<https://www.icevirtuallibrary-com.ezproxy.usq.edu.au/doi/full/10.1680/mobe.34525.0503>>.

Hosseinzadeh, N, Ghiasian, M, Andiroglu, E, Lamere, J, Rhode-Barbarigos, L, Sobczak, J, Sullivan Sealey, K, & Suraneni, P 2022, '*Concrete seawalls: A review of load considerations, ecological performance, durability, and recent innovations*', Ecological Engineering, vol.178, viewed 27 March 2023, <<https://www.sciencedirect.com/science/article/pii/S0925857422000349>>.

Hu, H & Liu, Y 2010, '*High modulus, high tenacity yarns*', Technical Textile Yarns, Woodhead Publishing, pp.329 – 286, accessed 5 September 2023, <[https://www.sciencedirect.com/science/article/abs/pii/B9781845695491500114#:~:text=High%20modulus%2C%20high%20tenacity%20\(HM%2DHT\)%20yarns%20are,%2DHT%20fibe rs%20%5B1%5D](https://www.sciencedirect.com/science/article/abs/pii/B9781845695491500114#:~:text=High%20modulus%2C%20high%20tenacity%20(HM%2DHT)%20yarns%20are,%2DHT%20fibe rs%20%5B1%5D)>.

Jabbar, S & Farid, S 2018, '*Replacement of steel rebars by GFRP rebars in the concrete structures*', Karbala International Journal of Modern Science, vol.4, viewed 6 May 2023, <https://www.researchgate.net/publication/323496303_Replacement_of_steel_rebars_by_GFRP_rebars_in_the_concrete_structures>.

Khorramian, K & Sadeghian, P 2017, '*Experimental and analytical behavior of short concrete columns reinforced with GFRP bars under eccentric loading*', Engineering Structures, vol.151, pp.761 – 773, accessed 6 September 2023, <<https://www.sciencedirect.com/science/article/pii/S0141029617320370>>.

Mackenzie, M 2017, 'Cyclone Debbie, three months on: How storm-hit towns in Queensland and NSW are recovering', ABC News, 9 July, viewed 29 April 2023, <<https://www.abc.net.au/news/2017-07-09/cyclone-debbie-three-months-on-how-storm-hit-towns-recovering/8666426>>.

Manalo, A, Alajarmeh, O, Yang, X, Ferdous, W, Ebrahimzadeh, S, Benmokrane, B, Sorbello, C, Weerakoon, S & Lutze, D 2022, 'Development and mechanical performance evaluation of a GFRP-reinforced concrete boat-approach slab', Structures, vol.46, pp.73-87, viewed 1 May 2023, <<https://www.sciencedirect.com/science/article/pii/S2352012422009377>>.

Maranan, G, Manalo, A, Benmokrane, B, Karunasena, Pm Mendis, P, & Nguyen, T 2019, 'Flexural behavior of geopolymer-concrete beams longitudinally reinforced with GFRP and steel hybrid reinforcements', Engineering Structures, vol.182, pp.141-152, viewed 8 August 2023, <<https://www.sciencedirect.com/science/article/pii/S0141029618305248>>.

McKenzie, A 2018, *Three yachts broke from their moorings at Bunbury's Koombana Bay Sailing Club*, Digital Image, ABC News, viewed 29 April 2023, <<https://www.abc.net.au/news/2018-06-05/power-out-homes-damaged-as-big-cold-front-threatens-wa/9834952>>.

NASA 2023, *Global Climate Change: Vital Signs of the Planet*, NASA's Jet Propulsion Laboratory, California Institute of Technology, California, viewed 26 March 2023, <<https://climate.nasa.gov/>>.

Othman, H & Marzouk, H 2016, 'An experimental investigation on the effect of steel reinforcement on impact response of reinforced concrete plates', International Journal of Impact Engineering, vol.88, pp.12-21, viewed 3 May 2023, <<https://www.sciencedirect.com/science/article/pii/S0734743X15001906>>.

Pullen, T, Allsop, N, Bruce, T, Kortenhaus, A, Schüttrumpf, H, & Van der Meer, J 2007, 'EurOtop wave overtopping of sea defences and related structures: assessment manual', Die Kuste, vol.73, pp.185, viewed 1 May 2023, <<https://documentatiecentrum.watlab.be/owa/imis.php?module=ref&refid=127303>>.

Ramakrishnan, K & Vinodhini, K 2019, '*Impact Testing on Reinforced Concrete Slab with Bfrp Bars as Reinforcement*', International Journal of Engineering and Advanced Technology, vol.8, no.6, viewed 3 May 2023, < <https://www.ijeat.org/wp-content/uploads/papers/v8i6/E7558068519.pdf>>.

Ruiz Emparanza, A, Kampmann, R & De Caso, B 2017, '*State-of-the-Practice of Global Manufacturing of FRP Rebar and Specifications*', ACI Fall Convention, viewed 5 May 2023, < https://www.researchgate.net/publication/327406172_State-of-the-Practice_of_Global_Manufacturing_of_FRP_Rebar_and_Specifications>.

Sadraie, H, Khaloo, A & Soltani, H 2019, '*Dynamic performance of concrete slabs reinforced with steel and GFRP bars under impact loading*', Engineering Structures, vol.191, pp.62-81, viewed 5 May 2023, < https://www.researchgate.net/publication/332720986_Dynamic_performance_of_concrete_slabs_reinforced_with_steel_and_GFRP_bars_under_impact_loading>.

Salih, Y, Abdulla, A & Muyasser, J 2022, '*Impact Resistance of GFRP Reinforced Concrete One-Way Slabs*', Information Sciences Letters, vol.11, pp.1267-1275, viewed 3 May 2023, < https://www.researchgate.net/publication/360901099_Impact_Resistance_of_GFRP_Reinforced_Concrete_One-Way_Slabs>.

Sheikh, S & Kharal, Z 2018, '*Replacement of steel with GFRP for sustainable reinforced concrete*', Construction and Building Materials, vol.160, pp.767-774, accessed 5 September 2023, < <https://www.sciencedirect.com/science/article/pii/S0950061817325461>>.

Shrivastava, A 2018, '*Plastic Properties and Testing*', *Introduction to Plastics Engineering, Plastics Design Library*, pp. 49-110, accessed 25 September 2023, < <https://www.sciencedirect.com/science/article/abs/pii/B9780323395007000034>>.

Siewert, T, Manahan, M, McCowan, C, Holt, J & Marsh, F 2002, '*The History and Importance of Impact Testing*', *American Society for Testing and Materials*, viewed 25 September 2023, < <https://www.nist.gov/publications/history-and-importance-impact-testing>>.

Tahmasebinia, F 2011, '*Reinforce Concrete Slabs Under Impact Loading*', Academic Publishing, third edition, viewed 24 July 2023, <https://www.researchgate.net/publication/269220230_Reinforced_Concrete_Slabs_Under_Impact_Loading>.

The Sun, 2017, *Shocking images show the destruction caused by the force of the powerful vessel*, Digital Image, The Sun, United Kingdom, viewed 29 April 2023, < <https://www.thesun.co.uk/news/3387936/huge-oil-spill-car-ferry-140-passengers-smashes-harbour-wall-gran-canaria/>>.

Wang, Z, Xie, J, Li, J, Liu, P, Shi, C & Lu, Z 2022, *'Flexural behaviour of seawater–sea sand concrete beams reinforced with GFRP bars: Effects of the reinforcement ratio, stirrup ratio, shear span ratio and prestress level'*, Journal of Building Engineering, vol.54, viewed 5 May 2023, < <https://www.sciencedirect.com/science/article/pii/S2352710222005794>>.

Xiao, Y, Bing, L & Fujikake, K 2017, *'Behavior of Reinforced Concrete Slabs under Low Velocity Impact'*, Aci Structural Journal, vol.114, viewed 4 May 2023, < https://www.researchgate.net/publication/311104384_Behavior_of_Reinforced_Concrete_Slabs_under_Low_Velocity_Impact>.

Yan, F, Lin, Z, Zhang, D, Gao, Z & Li, M 2017, *'Experimental study on bond durability of glass fiber reinforced polymer bars in concrete exposed to harsh environmental agents: Freeze-thaw cycles and alkaline-saline solution'*, Composites Part B: Engineering, vol.116, pp.406-421, accessed 6 September 2023, < <https://www.sciencedirect.com/science/article/pii/S1359836816315220> >.

Yang, X, Alajarmeh, O, Manalo, A, Benmokrane, B, Gharineiat, Z, Ebrahimzadeh, C & Weerakoon, S 2023, *'Torsional behavior of GFRP-reinforced concrete pontoon decks with and without an edge cutout'*, Marine Structures, vol.88, accessed 21 May 2023, < <https://www.sciencedirect.com/science/article/pii/S0951833922001812>>.

Yankelevsky, D 1997, *'Local Response of Concrete Slabs to Low Velocity Missile Impact'*, International Journal of Impact Engineering, vol.19, pp.331 – 343, viewed 23 July 2023, <https://www.researchgate.net/publication/222350847_Local_Response_of_Concrete_Slabs_to_Low_Velocity_Missile_Impact>.

Appendices

Appendix A – Project Specification

ENG4111/4112 Research Project

Project Specification

For: Megan Pretorius

Title: Performance Evaluation of GFRP bar diameters in Reinforced Concrete Slabs Subjected to Impact Loads.

Major: Civil Engineering

Supervisors: Dr Allan Manalo & Dr Omar Alajarmeh

Enrollment: ENG4111 – EXT S1, 2021

ENG4112 – EXT S2, 2021

Project Aim: The aim of this project is to investigate and evaluate the structural performance of different diameters of Glass Fiber Reinforced Polymer (GFRP) bars in concrete slabs when subjected to impact loads. This investigation aims to apply its findings to improve the performance of reinforced concrete seawalls in Australia.

Programme: Version 1, 15th March 2023

Example below

1. Conduct initial background into seawalls, the properties of GFRP bars and the structural behavior of impact loads on traditional reinforced concrete slabs.
2. Conceptualize a suitable configuration to drop a weight onto GFRP reinforced concrete slabs.
3. Seek scheduled access to USQ testing facilities (P11 & P2) and complete safety induction.
4. Check to see what material resources are available and what needs to be procured.
5. Construct drop weight frame for testing and GFRP reinforced concrete test samples.
6. Select and assess hardware used for recording of results.
7. Begin the testing phase for all specimens.
8. Process and evaluate the experimental data recorded.
9. Make relevant conclusions from the results achieved.

If time and resource permit:

10. Complete an experimental modelling simulation using Strand7 software to increase depth of analysis.

Appendix B – Project Resources

ENG4111/4112 Research Project

Project Resources

For: Megan Pretorius

Title: Performance Evaluation of GFRP bar diameters in Reinforced Concrete Slabs Subjected to Impact Loads.

Supervisors: Dr Allan Manalo & Dr Omar Alajarmeh

Material Resources:

- Sourcing of 20 x Glass Fiber Reinforced Polymer bars for each diameter of 8mm, 10mm and 13mm (Total of 60 GFRP bars).
- Sourcing of 20 x 20mm steel reinforcement bars.
- Sourcing 50MPa concrete.
- Sourcing of correct PPE for laboratory testing.

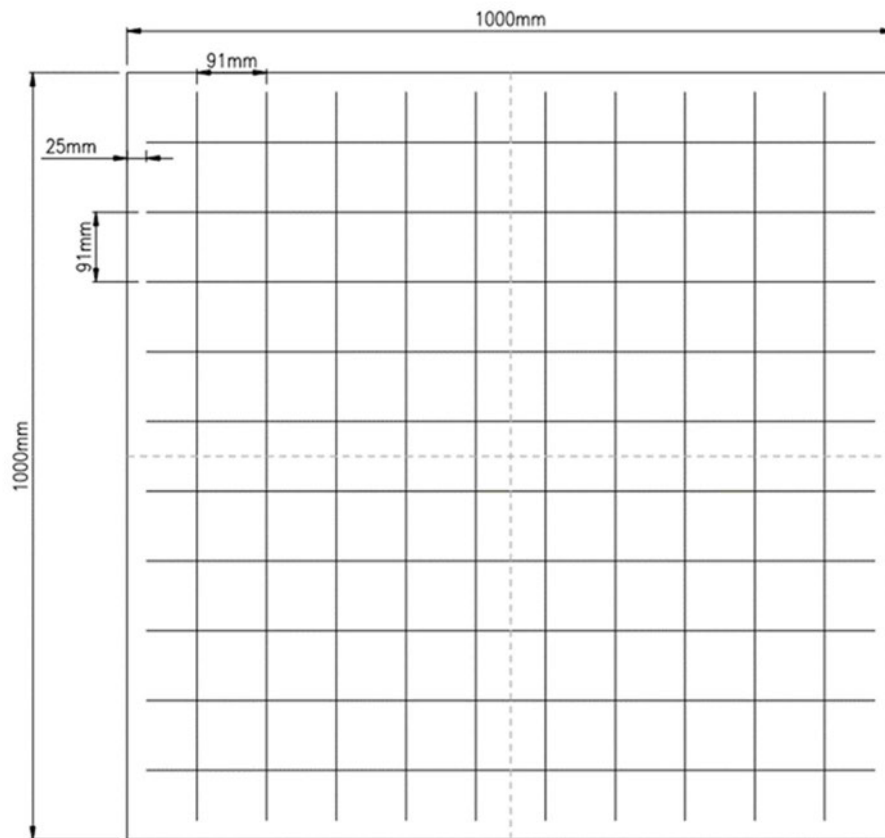
Machine & Laboratory Resources:

- Access to USQ Engineering Testing Facilities (P11 & P2).
- Access to hardware used for recording of results.

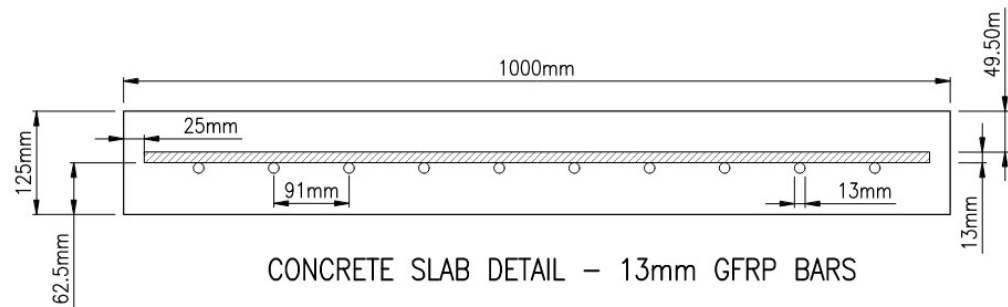
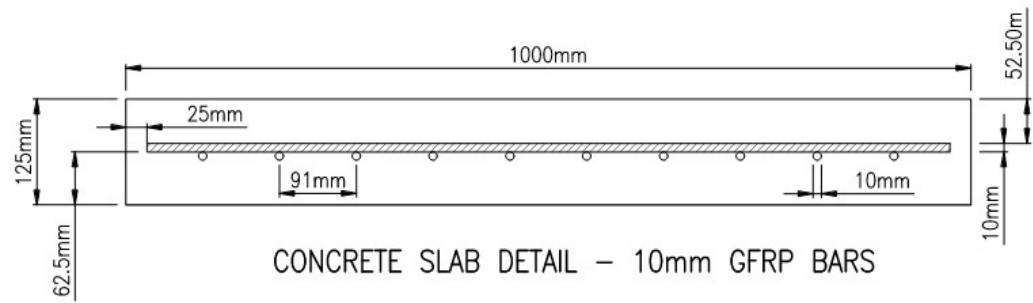
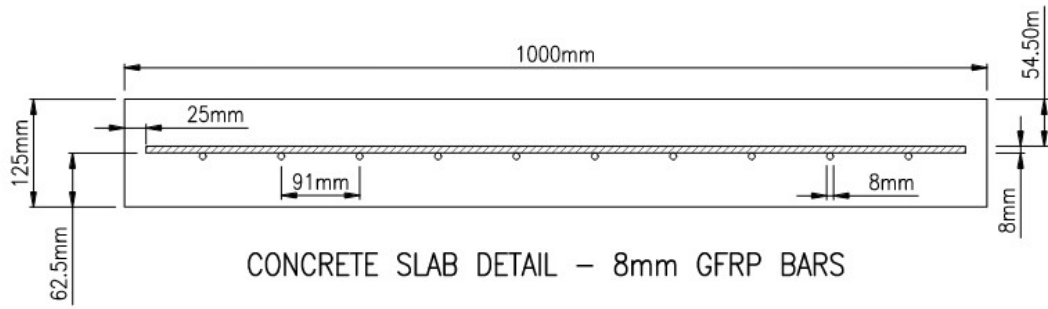
Contingencies for problems:

- Laboratory work will be conducted under the supervision of experienced technical officers to avoid problems from occurring during the testing process.


Appendix C – Internal Reinforcement Configurations



TYPICAL CONCRETE SLAB DETAIL



Appendix D – Risk Assessment

NUMBER	RISK DESCRIPTION	TREND	CURRENT	RESIDUAL
2088	Impact loading test for GFRP reinforced concrete seawalls		Low	Low
DOCUMENTS REFERENCED				
Drop weight test instructions				
RISK OWNER	RISK IDENTIFIED ON	LAST REVIEWED ON	NEXT SCHEDULED REVIEW	
Ezgi Bal Yetim	05/03/2023	20/03/2023	20/03/2024	
RISK FACTOR(S)	EXISTING CONTROL(S)	PROPOSED CONTROL(S)	OWNER	DUE DATE
Bodily injury due to overstraining or contact with rough edges	<p>Control: Use a lifting truck/forklift available to carry 14 specimens from P8 to P11. Follow the proposed lifting procedure by the lab technician. Do not manually lift the concrete slabs. Place them to the secured place.</p> <p>Control: Wear rigging gloves and safety shoes</p> <p>Control: If it is necessary to handle or move concrete slabs on the floor, mechanical aids should be used, otherwise, a sufficient number of people are required.</p>	No Control:		
Improper Operation/Use or Overloading of forklifts can cause collisions, injuries, fatalities, and product and equipment damage.	<p>Control: Ensuring all forklift operators hold a valid forklift licence and have completed up to date training. All operators are aware of the units maximum safe load limit via its rating plate and should behave professionally.</p> <p>Control: Install safety measures such as guard rails and line markings to separate machines and pedestrians in the lab. Also, use of</p>	No Control:		

	<p>install spotlights and horns on forklifts to alert pedestrians to the unit's presence.</p> <p>Control: Stand clear of the forklift pathway and remove pedestrians.</p>	
Wet and slippery floors can cause a forklift to skid, whilst cracks and pot holes in the ground can cause the unit to tip over.	<p>Control: Before the operation, any wet and slippery hazards should be cleaned up, debris and obstructions removed and cracks and pot holes should be fixed to ensure a safe work environment for forklifts to operate over.</p>	No Control:
Falling of concrete seawalls (300 kg) to the ground accidentally which can cause serious crushing injury	<p>Control: One seawall weighs around 300 kg. To place the seawalls on the supports, the lab technician should use a forklift or lifting truck to lift samples. Do not manually lift.</p> <p>Control: Keep clear with barriers, signage and/or spotters during the testing. Stand clear of the testing area. Do not stand under the frame. Wait until the testing has been completed.</p> <p>Control: Always wear safety shoes and helmet.</p>	No Control:
Falls of workers from height leading cause of death and serious injury	<p>Control: Make sure there is a fall prevention device such as barriers, scaffolding, and elevating work platforms.</p> <p>Control: People working at heights over two metres must hold working at heights licence or be directly supervised by someone who does.</p> <p>Control: Wear safety helmet at all times.</p>	<p>Control: Could be added an industrial rope access system or a safety net or catch platform.</p> <p>17/03/2023</p>

Large drop hammer weight (300 kg) falls unexpectedly due to not connecting rigging or seacatch appropriately - damage to test setup by rigging slippage and serious injury to the human body	<p>Control: Proper rigging should be employed. Ensure seacatch locking pin is inserted. Check Rigging for twists and rectify, and ensure shackles are tight. All operations should be checked by lab technicians.</p> <p>Control: Make sure the lifting sling is sturdy. Only a lab technician is authorized to do and check the attachments. Follow the pre and post checks documented in the instructions.</p> <p>Control: Erect barriers around the test site to prevent people entering the hazardous area. Vacate the test exclusion zone.</p>	<p>Control: Conduct trials with low mass weight in a safe environment to confirm the function of the quick-release catch before using the full 300 kg weight.</p> <p>20/03/2023</p>
Hoist drop hammer into guide tube incorrectly - damage to test setup by rigging slippage (Min 2 people required)	<p>Control: Drop weight should be lifted and positioned centrally inside the guide tube by the crane operator. (Personnel Member 1)</p> <p>Control: Seacatch rope assembly should be continually adjusted during the lift to prevent snagging (Personnel Member 2). If Rope Snag occurs stop and Re-evaluate from the outside exclusion zone immediately.</p> <p>Control: Ensure elevation of drop weight is not above the point where the tip is parallel with the top of the upper guide tube viewing slot. When lift is complete, rope/string is held by one personnel until setup is complete.</p> <p>Control: Watch warning lights and signage at workshop entry points.</p>	<p>No Control:</p>
Exposure to Loud noise, dust and eyes due to concrete pieces splashing around during the impact	<p>Control: A protection screen will be placed between the personnel and</p>	<p>Control: Place some vibration-damping materials (such as rubber mats/pads) to</p> <p>17/03/2023</p>

test	<p>the test machine.</p> <p>Control: Wear safety glasses for eye protection, hearing protection and masks at all times.</p>	<p>reduce vibration transmission to the surrounding area.</p> <p>Control: Install several soundproofing materials surrounding the testing area/steel frame, such as acoustic foam or soundproof panels, to reduce the amount of noise.</p> <p>17/03/2023</p>
------	--	---